Electrochemical Energy Reviews (2023) 6:28
https://doi.org/10.1007/s41918-023-00190-w

REVIEW ARTICLE

Recent Advances on PEM Fuel Cells: From Key Materials to Membrane Electrode Assembly

Shanyun Mo[1,2] · Lei Du[1] · Zhiyin Huang[1] · Junda Chen[1] · Yangdong Zhou[1] · Puwei Wu[1] · Ling Meng[1] · Ning Wang[1] · Lixin Xing[1] · Mingquan Zhao[2] · Yunsong Yang[2] · Junke Tang[2] · Yuquan Zou[2] · Siyu Ye[1,2]

Received: 3 September 2022 / Revised: 14 December 2022 / Accepted: 2 April 2023 / Published online: 17 August 2023

Abstract
In recent years, proton exchange membrane (PEM) fuel cells have regained worldwide attention from academia, industries, investors, and governments. The prospect of PEM fuel cells has turned into reality, with fuel cell vehicles successfully launched in the market. However, today's fuel cells remain less competitive than combustion engines and batteries, primarily due to their high cost and short lifetime, which are significantly affected by the membrane electrode assembly (MEA), or the "chips" of PEM fuel cells. Therefore, many efforts have been devoted to developing advanced materials and manufacturing processes for MEAs. In this paper, we critically review the recent progress of key materials for MEAs, focusing on how to integrate materials into electrodes and MEAs. We also present the most advanced designs and manufacturing techniques of MEAs and discuss their possible constraints. Finally, perspectives on future R&D directions of materials and MEAs are provided. This review aims to bridge the gaps between academic material research and industrial manufacturing process development.

Keywords Materials · Manufacturing · Membrane fuel cell · Membrane electrode assembly

1 Introduction

Proton exchange membrane (PEM) fuel cells are one of the most promising technologies toward achieving "carbon peak and neutrality" goals. While PEM fuel cells have risen and declined in recent centuries, they presently play a key role in building a sustainable society [1]. Today's PEM fuel cells offer a much lower Pt loading compared to early-stage iterations. For example, the total Pt loading of the first-generation Toyota Mirai fuel cell (2017, the first commercialized PEM fuel cell vehicle) was only 0.365 mg_{Pt} cm^{-2}, greatly improving upon the first "practical" fuel cell (1962, 35 mg_{Pt} cm^{-2}) which used potassium hydroxide solution as the electrolyte. The great progress of PEM fuel cells is attributed not only to the development of Pt electrodes, but also to the replacement of conventional acidic/alkaline solutions with advanced perfluorosulfonic acid membranes (e.g., Nafion) as launched in the 1970s, as well as development of the membrane electrode assembly (MEA) structure and related manufacturing processes.

PEM fuel cells have been gradually deployed in commercial applications, e.g., as the power source for vehicles [2]. Toyota, Hyundai, and Honda have all launched fuel cell vehicles in the market. One representative example is the second-generation Toyota Mirai fuel cell stack (2020), which has demonstrated excellent power density of 5.4 kW L^{-1} (vs. 3.1 kW L^{-1} for the first generation) and represents a milestone in the history of PEM fuel cells. However, PEM fuel cells are currently less competitive than combustion engines and batteries, which is primarily attributed to their high cost and short lifespan. To overcome these barriers, advanced materials and developed manufacturing technologies are required. Such advancement will require close collaboration between enterprises,

Shanyun Mo and Lei Du have contributed equally to this work.

✉ Lixin Xing
lixinxing@gzhu.edu.cn

✉ Siyu Ye
siyu.ye@gzhu.edu.cn

[1] Huangpu Hydrogen Energy Innovation Centre/School of Chemistry and Chemical Engineering, Guangzhou University, Guangzhou 510006, Guangdong, China

[2] SinoHykey Technology Company Ltd., Guangzhou 510760, Guangdong, China

universities, research institutes, customers, and governments. During this process, fundamental research should be focused on developing a high-performing and durable MEA—the "chip" of PEM fuel cells—while industrial efforts should consider the scaled-up production of the key materials and components.

At present, the performances of MEA components, including catalysts, ionomers, membranes, gas diffusion layers, etc., have been significantly improved, and mature materials have been successfully applied in industry. However, integrating these materials into an MEA usually leads to significant performance losses. The technical community has given much attention to the compatibility of the components and therein developed better MEA manufacturing processes. Herein, this review provides an overview of the development of key materials and manufacturing processing for MEA, in support of minimizing gaps between the fundamental research in materials and the manufacturing process in industry.

2 Recent Progress in Key Materials for MEA

An integrated MEA houses the primary electrochemical reactions and plays a central role in PEM fuel cells, which usually consist of at least six primary components, including the catalyst, ionomer, proton exchange membrane, gas diffusion layer, binder, and frame, as shown in Fig. 1a, b. An illustration of the working mechanisms in the MEA is given in Fig. 1c. The electric energy is generated by separate redox reactions at the anode and cathode of MEAs, as illustrated in Eqs. 1–3.

$$\text{Anode: } H_2 = 2H^+ + 2e^- \quad (1)$$

$$\text{Cathode: } O_2 + 2H^+ + 2e^- = H_2O \quad (2)$$

$$\text{Overall reaction: } H_2 + O_2 = H_2O \quad (3)$$

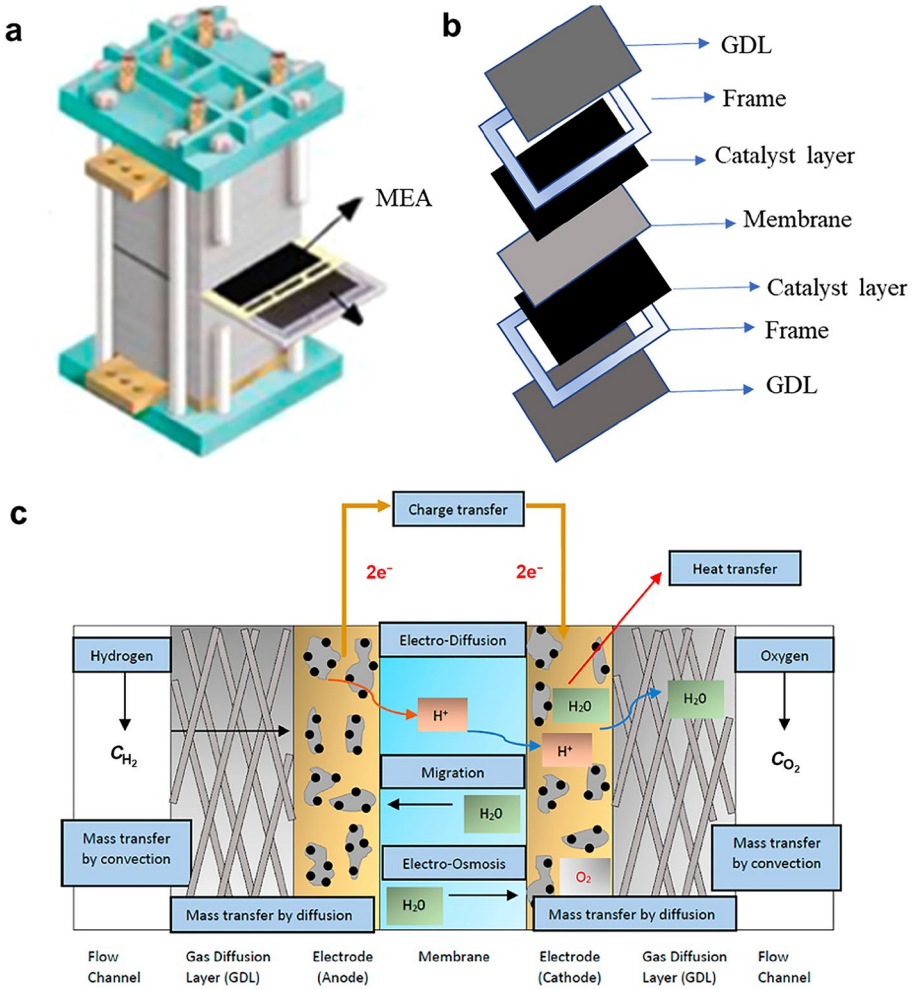

Fig. 1 **a** An illustration of a PEM fuel cell stack. Reprinted with permission from Ref. [10]. Copyright © 2019, Elsevier Ltd. **b** The key materials in an integrated MEA. **c** An illustration of working mechanisms in MEA. Reprinted with permission from Ref. [11]. Copyright © 2021, Elsevier Ltd

Therefore, superior kinetics for these redox reactions is highly desired. This requires highly efficient catalysts, which can remarkably accelerate reaction kinetics. Usually, catalysts work in a so-called catalyst layer, which is located between the gas diffusion layer (GDL) and the proton exchange membrane. To facilitate proton transfer in the bulk catalyst layer and enhance the mechanical strength of the catalyst layer, an ionomer with proton conductivity (also the ability to serve as a binder) is needed. The composition of the ionomer is usually the same as that of the membrane, which allows fast proton transfer from the anode to the cathode and prevents hydrogen and oxygen crossover during operation. In addition, hydrophobic GDLs on the catalyst layers of both sides are crucial to distributing gases and remove excess water, i.e., water management in fuel cells. Reasonably, the abovementioned materials represent cores for an MEA. We emphasize that they are somewhat soft, so the derived MEA is not sufficiently strong with respect to its mechanical properties [3]. In this regard, the outer frames are employed to provide a firm and reliable MEA structure [4, 5] and are also used as seals. In this configuration, binders cohering to the frame are applied [6–9]. These key materials significantly determine the performance and lifetime of MEAs. In the following sections, we will discuss the most recent progress in these key materials, particularly those that are mature and have been widely applied in the MEA industry.

2.1 Catalysts

An MEA consists of an anode and cathode, which provide sites for the hydrogen oxidation reaction (HOR, Eq. 1) and oxygen reduction reaction (ORR, Eq. 2), respectively. For both the anodic HOR and cathodic ORR, Pt-based materials are the most popular catalysts, which have been widely used in commercialized PEM fuel cells and as the benchmark against which research and development is evaluated [12–14]. Due to the fast HOR, the required amount of Pt-based catalyst at the anode is quite low, e.g., 0.05 mg cm^{-2} [15, 16]. In contrast, the cathodic ORR kinetics is much lower than the HOR kinetics, thus requiring much more Pt catalysts than the anode and primarily leading to increased cost [17, 18]. For example, the anode Pt loading for the Mirai fuel cell is only 0.05 mg_{Pt} cm^{-2} while that for the cathode is up to 0.315 mg_{Pt} cm^{-2} [19, 20]. Meanwhile, ORR works under harsher and highly oxidative environments, thus suffering from fast degradation. Generally, cathode catalysts are the primary bottleneck for an MEA and have been intensively studied [21]. In this section, we primarily focus on the progress of the cathode catalyst development. This does not signify that the anode catalyst is not important—at the anode, reactive oxygen species are likely to be generated under inappropriate operation (e.g., H_2 starvation, start-up/shut-down and reversal), leading to aggressive material degradation (e.g., membrane and ionomer) [22].

The most popular catalysts for ORR are Pt-based materials because Pt intrinsically offers a good ability to activate oxygen molecules and is relatively stable under harsh ORR conditions. To reduce the Pt loading at the cathode, intrinsic activity for Pt-based catalysts needs improvement. To date, various strategies to improve the performance have been developed, such as alloying Pt with transition metals [23, 24], building the core–shell structure [25, 26], nanowires [27–29], nanoplates [30], and nanoframes [31, 32]. As a milestone for Pt-based ORR catalysts, Duan et al. successfully built jagged Pt nanowires (J-Pt NWs) through annealing–dealloying. Per the high electrochemical active surface area of one-dimensional materials, the ECSA of J-Pt NWs was successfully increased to up to 118 m^2 g^{-1}; in particular, the mass activity tested by rotating-disk-electrode (RDE) reached an ultrahigh value of 13.6 A mg_{Pt}^{-1} at 0.9 V [33].

The alloying of Pt with other metal(s) is the most widely employed strategy for catalyst design [34]. The d-band center of Pt sites has been widely accepted as a descriptor for ORR intrinsic activity [35–37]. A high d-band center benefits the adsorption of oxygen-containing species but leads to slow intermediate desorption and active site poisoning, while a low d-band center suffers from slow adsorption of oxygen and low kinetics [37, 38]. Therefore, alloying Pt with other transition metals such as Co and Ni could moderate the d-band center of Pt active sites and present fast kinetics (Fig. 2). In addition, the introduction of transition metals remarkably decreases the percentage of Pt in the nanoparticles, thus lowering Pt usage. For example, Liu et al. loaded PtCo alloying nanoparticles on Co–N–C substrates, and the synergistic alloying effect and ligand effect significantly accelerated the ORR process on PtCo active sites. DFT calculations demonstrate that the elution and attachment characteristics of oxygenates are well adjusted on the active sites during the reaction, which efficiently reduces the intermediate into H_2O and cuts off the pathway to producing undesired H_2O_2 and/or free radicals [39]. Recently, intermetallic compounds have shown great promise in ORR due to their unique highly ordered nanostructures. Distinct from conventional alloys with random atom arrangements, intermetallics can provide high concentrations of well-defined active sites for ORR, as well as extremely high stability under harsh working conditions [40, 41]. One of the major challenges for synthesizing intermetallics is their large diameter after high-temperature annealing, which leads to a decreased surface area. In this regard, an efficient sulfur-anchoring strategy was proposed to control the Pt-based intermetallic size to < 5 nm after up to 1 000 °C sintering [42]. In particular, the ORR mass activity of this intermetallic catalyst reached 1.3–1.8 A mg_{Pt}^{-1} at 0.9 V.

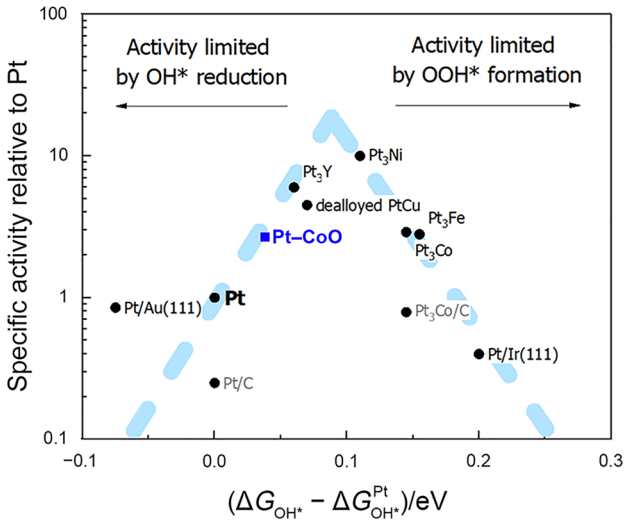

Fig. 2 Volcano plot showing experimental activity data from electrochemical RDE measurements at 0.9 V (vs. RHE) relative to Pt as a function of the hydroxyl intermediate binding energy ΔG_{OH^*}. Reprinted with permission from Ref. [43]. Copyright © 2021, Springer Nature

In addition to the significant progress in Pt-based catalysts for ORR, a large number of efforts have been devoted to Pt-group-metal-free (PGM-free) catalysts, which are promising alternatives to replace costly and scarce Pt catalysts [44, 45]. Among various PGM-free catalysts, composites involving so-called single-atom moieties are emerging [46], i.e., transition metal–nitrogen–carbon (M–N–C) catalysts. Over the past decades, several kinds of PGM-free catalysts have been developed, among which the most representative is Fe–N–C due to its superior activity as a site for ORR [47]. In alkaline media, the most advanced Fe–N–C catalyst has presented superior ORR activity to Pt-based catalysts; however, it remains less competitive than Pt in terms of activity and stability in acidic media, i.e., in PEM fuel cells [48–50]. To improve the activity of the Fe–N–C catalyst, building well-defined and highly utilized atomically dispersed Fe–N_x moieties is essential [51]. By tuning the content of doped Fe into zeolitic imidazolate framework (ZIF)-8 precursors, exclusively atomically dispersed FeN_4 sites have been achieved, which present a significantly improved active site density and half-wave potential ($E_{1/2}$) of (0.88 ± 0.01) V vs. RHE [52]. Recently, dual single-atom catalysts were proposed to achieve better ORR intrinsic activity, e.g., Fe/Co–N–C [53, 54].

To efficiently screen and develop desired M–N–C catalysts, an artificial intelligence (AI)-assisted strategy has emerged to address the challenges of tedious and laborious experimental activities. As shown in Fig. 3a, b, a reliable ensemble learner, XGBoost, was established and trained to rank the degrees of importance among 26 complicated features in PEM fuel cells. The artificial neural network (ANN) is the most accurate machine learning algorithm and has suggested that the backpressure, cathodic loading amount and BET surface area are the most important parameters for PEM fuel cell operation and cathode catalysts (Fig. 3b). Note that these AI strategies have been widely applied in fuel cell research and development [55, 56], in addition to the catalysts mentioned above.

Despite the improved ORR activity, the instability issue of PGM-free catalysts has been specifically highlighted in recent years [58, 59]. For the high-performing Fe–N–C catalysts, demetallation and carbon corrosion may be the most likely degradation mechanisms [48]. Many strategies have been proposed to enhance the stability of Fe–N–C catalysts, as discussed in Ref. [60]. Recently, by depositing a thin layer of nitrogen-doped carbon on the NH_4Cl-treated Fe–N–C catalyst, the catalyst stability was markedly enhanced because a substantial proportion of stable S2 sites were synthesized [59]. In particular, the dissolved and even undissolved Fe from Fe–N–C catalysts is vulnerable to H_2O_2 and generates highly oxidative radicals via Fenton reactions (Eqs. 4–6).

$$Fe^{2+} + H_2O_2 \rightarrow Fe^{3+} + OH^- + OH\cdot \quad (4)$$

$$H_2O_2 + Fe^{3+} \rightarrow Fe^{2+} + O_2 + 2H^+ \quad (5)$$

$$O_2 + Fe^{2+} \rightarrow Fe^{3+} + O^{2-} \quad (6)$$

The oxidation potential of the peroxyl radical is approximately 1.3 V, so OH· likely dominates as the main radical product, which is quite harmful to not only the catalysts but also other MEA components, e.g., ionomers and membranes. In this regard, Fe-free M–N–C catalysts, including Co–N–C and Mn–N–C, have been proposed, which have presented better stability but still suffer from low ORR intrinsic activity [61]. In addition, metal-free catalysts, i.e., doped carbon matrices by heteroatoms such as N, S, O, and F, have also been studied [62–64]. Although milestones have been achieved in terms of PGM-free catalysts, there is still a gap between their stability and activity compared to Pt-based catalysts. In other words, PGM-free catalysts are not mature enough to be applied in real-world MEAs, particularly for automotive applications.

Another note is that the reported ORR activity of catalysts in the literature is mostly evaluated by the three-electrode system, i.e., RDE, rather than in the MEA, which is more relevant to fuel cells. However, not all RDE activity can be well reproduced in the MEA (Fig. 4). Actually, the activity in MEA is more important than in the RDE. The US Department of Energy (DOE) targets for PEM fuel cells are all based on MEA performance. The performance gap of the same catalyst as evaluated by RDE and MEA should be

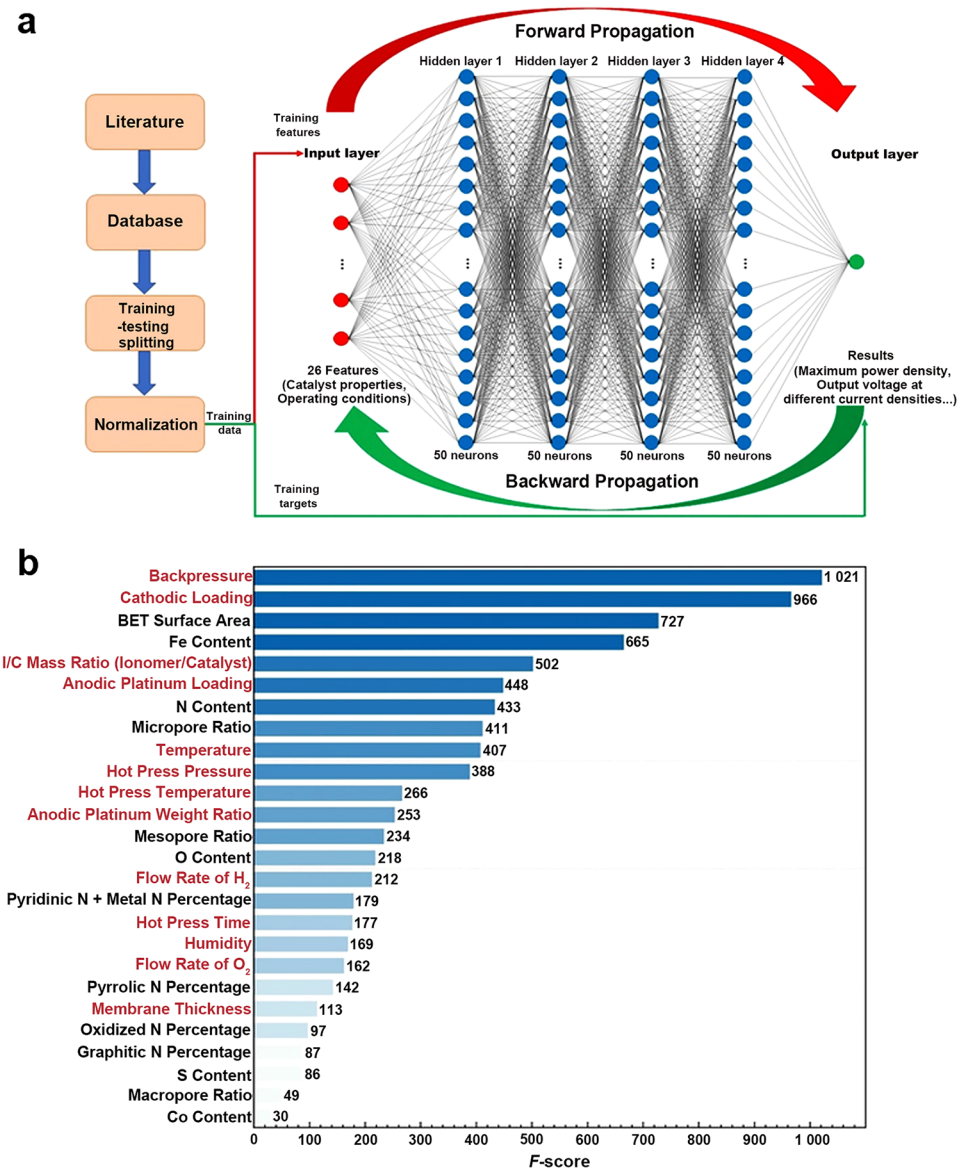

Fig. 3 **a** Illustration of the artificial neural network (ANN). **b** Feature importance heuristic given by the XGBoost algorithm (red features are correlated with PEM fuel cell operating conditions, and black features are correlated with the intrinsic properties of catalysts). Reprinted with permission from Ref. [57]. Copyright © 2020, Wiley–VCH GmbH

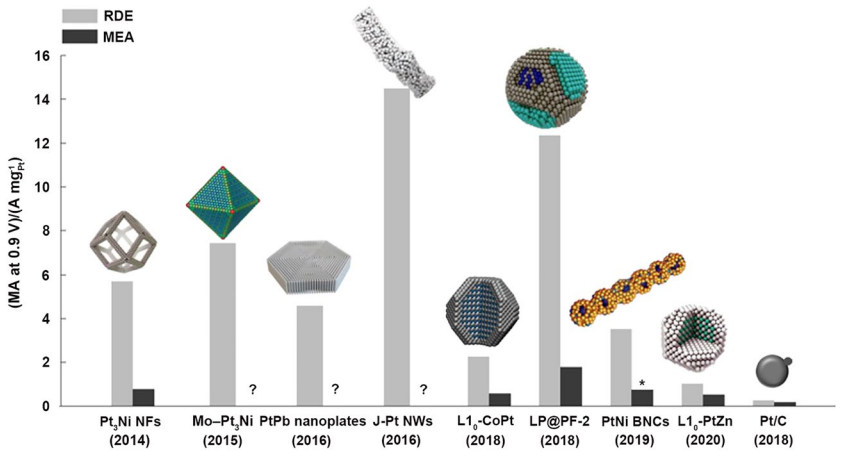

Fig. 4 The ORR activity and stability of the state-of-the-art novel Pt-based nanocatalysts achieved in labs far exceed commercialized Pt/C at RDE levels. It is very difficult to draw conclusions on expected MEA-level activities based on such seemingly impressive RDE performance because RDE and MEA tests are substantially different. Reprinted with permission from Ref. [66]. Copyright © 2021, Springer Nature

attributed to their different features. For example, the RDE method is performed in a liquid electrolyte where the solubility of O_2 is low. To facilitate the O_2 supply, forced convection (rotating) and a thin catalyst film (usually < 1 μm) are both needed. In this situation, the resistance to oxygen transfer is eliminated, and the intrinsic kinetics parameters (e.g., the activity at 0.9 V) be obtained in a low-current–density region (normally 10 mA cm^{-2}). In contrast, in an MEA configuration, the catalyst layer is thick and complicated in composition and structure. Under this situation, the oxygen transfer resistance cannot be ignored, which leads to significant performance loss at high current densities > 1 A cm^{-2}, especially when the Pt loading is low [65]. In this regard, screening catalysts by RDE and then evaluating ORR activity in MEA may be a good and necessary choice. Reasonably, decreasing the gaps between RDE and MEA by designing catalysts is an essential task in this field [66]. To improve MEA activity, decreasing the oxygen transfer resistance (particularly the local O_2 transport resistance) is important. Several strategies can be considered to address the oxygen transfer issue in MEAs. On the one hand, Pt-based catalysts with large electrochemical surface areas are desired to ensure O_2 transport to the Pt surface at high current densities, so research efforts at the catalyst level should be focused on the electrochemical surface area in addition to the mass/specific activity. On the other hand, structure engineering in interior pores and surface modification can promote Pt particle dispersion, reduce ionomer coverage, force ionomers to be homogeneously distributed and lower the local O_2 transport resistance.

2.2 Membranes and Ionomers

The proton exchange membrane in MEA provides channels for proton migration and transmission, separates gas reactants, and isolates electron transfer [67, 68]. At the same time, the ionomer plays an important role in distributing protons across the whole catalyst layer. In this regard, the function of the ionomer is partially the same as that of the membrane. Therefore, we discuss the progress of both membranes and ionomers in this section.

Membranes (proton exchange membrane, PEM, to be specific), as one of the most important components of PEM fuel cells, significantly determine the working temperature, ohm resistance, service life, and thus the comprehensive performance of PEM fuel cells [69]. According to the US DOE, the membrane occupies 17%, 12%, and 9% of the total cost, respectively, if the fuel cell circulation reaches 1 000, 10 000, and 50 000 per year [70]. The general requirements for PEMs include high ionic conductivity, low air permeability, good thermal stability, electrochemical stability, excellent mechanical properties in dry and hydrated states, an adequate water absorption rate, and a moderate swelling rate. Nafion series perfluorosulfonic acid (PFSA) membranes produced by DuPont (now by Chemours) are the most widely used membranes for PEM fuel cells due to their high proton conductivity and high thermal and mechanical stability [71]. The PFSA molecule is composed of a polytetrafluoroethylene (PTFE) main chain, perfluoroethylene side chain, and sulfonic acid group [72]. The PTFE main chain is hydrophobic and determines the mechanical and chemical stability of the proton exchange membrane [73]. The sulfonic acid end groups are the primary active components for proton conductivity.

Due to the different side chain lengths, PFSA membranes can be divided into long side chain (LSC) membranes and short side chain (SSC) membranes [74–76]. The former is represented by Nafion film [77], while the SSC PFSA was launched by Dow Chemical in the last century, albeit at a higher cost than LSC PFSA. The molecular structures of these two types of PFSA membranes are shown in Fig. 5a, b. In 2010, Solvay–Solexis produced and launched the Aquivion SSC membrane. Compared with the Nafion LSC membrane, Aquivion SSC membranes show higher ionic conductivity, higher water absorption, similar mechanical properties, and higher glass transition

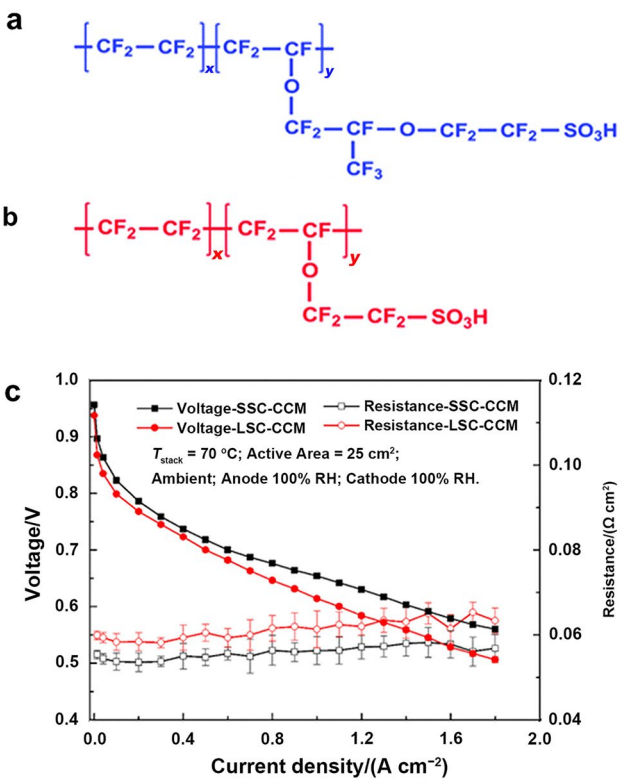

Fig. 5 **a** Molecular structures of LSC PFSA, **b** molecular structures of SSC PFSA. Reprinted with permission from Ref. [76]. Copyright © 2021, Springer. **c** Polarization curves and HFR of the CCMs prepared by SSC PFSA and PFSA ionomers. Reprinted with permission from Ref. [78]. Copyright © 2020, American Chemical Society

temperature [78] to therefore present better performance in MEA, particularly at low humidity (Fig. 5c). Notably, the water content of SSC membranes is significantly larger due to their much higher ion exchange capability (IEC), which indicates that the network of hydrophobic channels is poorly developed compared to LSC analogues. In the past, thicker PFSA membranes (e.g., 180 μm Nafion N117 or 120 μm Nafion N115) were widely used in PEM fuel cells, which offer good mechanical strength and low gas permeation but low proton conductance due to their large thickness. At present, PFSA membranes may be less than 10 μm and have shown significantly improved proton conductance and lower ohmic losses, which, however, suffer from high gas crossover. A thinner membrane can lead to reduced Faraday efficiency, accelerated degradation, and even safety risks.

During PEM fuel cell operation, the proton conductivity of the membrane is always affected by temperature and humidity. Usually, low temperature and high humidity benefit the proton conductivity of the PFSA membrane. PFSA membranes demonstrate excellent proton conductivity at 80–90 °C in humidity [79]. In contrast, increased temperature is always preferred for fuel cell operation because high kinetics, energy efficiency, and output power can be obtained. Moreover, catalysts suffer from less CO-induced degradation at high temperatures [80–83]. Another benefit at high temperatures is that PEM fuel cells offer easier heat and water management. These optimal working conditions for fuel cells are actually not conducive to good operation of PFSA membranes. For example, a high working temperature will lead to membrane degradation and failure due to dehydration. On the other hand, when PEM fuel cells are stored in cold environments (cold regions), some of the water is confined in the polymer chain, which is readily frozen on the membrane surface. Once frozen PEM fuel cells are directly initialized, pinholes easily form on the membrane surface [84, 85]. Therefore, a type of membrane that is propitious to a wide temperature range, especially at high temperatures, is crucial for future PEM fuel cell development [86].

To develop advanced membrane materials for high working temperatures, several efficient strategies have been proposed. The modification of conventional PFSA membranes is an efficient technique to improve the high-temperature properties, for example, tuning the acid groups in PFSA molecules, including: (1) increasing acid group concentration and changing the position of sulfonic acid groups, which is beneficial for proton conductivity; (2) building multiblock copolymers with long hydrophilic/hydrophobic blocks and/or copolymers with locally high sulfonic acid group concentration to increase proton conductivity; (3) developing branched polymers; (4) filling polymers into porous substrates with high strength; (5) doping hydrophilic additives into the polymers; (6) incorporating polymers with water-free acid, ionic liquid, heteropoly acids, triazole or imidazole; and (7) fabricating polymers nanofibers to reinforce the membrane [87]. In addition, new types of membrane materials have been developed for high working temperatures, including sulfonated hydrocarbon polymers, e.g., sulfonated derivatives of poly(arylene ether)s (SPAEs), poly(arylene sulfide)s (SPASs), polyimides (SPIs), polybenzimidazoles (PBIs), polyphenylenes (PPs) and their composite membranes (Fig. 6a, b). These materials can be synthesized from diverse monomers via various routes to obtain a variety of structural architectures [88]. Particularly for high-temperature PEM fuel cells, phosphoric acid (H_3PO_4, PA)-doped PBI membranes have been widely used without humidification due to their low cost and excellent chemical and thermal properties in the temperature range from 100 to 250 °C. PA has proven to be a superior dopant because the derived membranes always offer high conductivity, excellent thermal stability, and very low vapor pressure at high temperatures. For example, Tang et al. studied the properties of a PA-doped ultra-porous membrane, which can operate in the temperature range of − 20–200 ℃. The membrane can also maintain a high retention rate of PA under the condition of high humidity, and the proton conductivity is three orders of magnitude higher than that of the traditional high-density PA-doped polybenzimidazole membrane. Usually, a

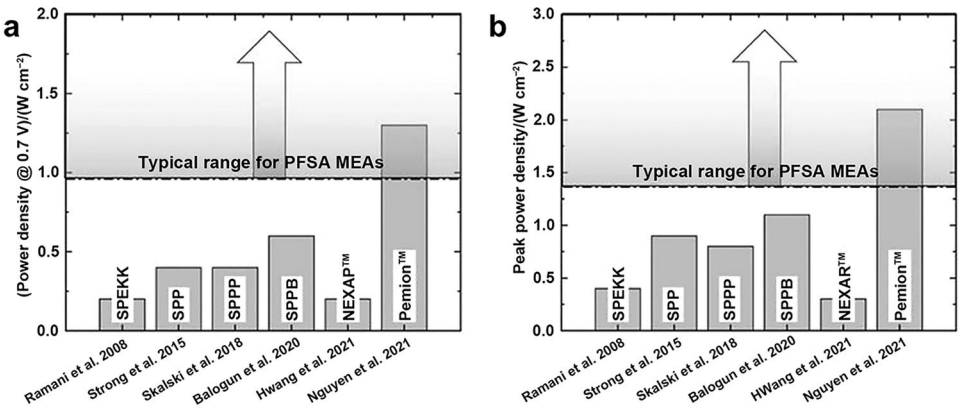

Fig. 6 **a**, **b** Power density at 0.7 V and peak power density in H_2/O_2 operation conditions, high humidity (> 75%), and ambient pressure reported in the literature based on fully hydrocarbon MEAs since 2008. Reprinted with permission from Ref. [68]. Copyright © 2022, Wiley–VCH GmbH

nonhumidified PA-doped membrane operates at 140–180 °C to avoid PA leaching caused by water condensation [79].

Proton transfer within polymer matrices often follows two possible mechanisms: vehicular and Grotthuss mechanisms. The vehicular mechanism refers to proton diffusion and migration in the form of a hydronium ion (H_3O^+) through the aqueous medium. On the other hand, the Grotthuss mechanism refers to proton hopping between water molecules by hydrogen bonding [89]. It is generally accepted that proton conduction in PA-doped PBI membranes primarily follows the Grotthuss hopping mechanism, as illustrated in the following equations [90].

$$\text{Anode: } H_2PO_4^- + H^+ \rightleftarrows H_3PO_4 \tag{7}$$

$$\text{Membrane}: H_3PO_4 + \text{PBI} \rightleftarrows H_2PO_4^- + \text{PBI} \cdot H^+ \text{ or } H_3PO_4 + H_2O \rightleftarrows H_2PO_4^- + H_3O^+ \tag{8}$$

$$\text{Cathode: } \text{PBI} \cdot H^+ \rightleftarrows \text{PBI} + H^+ \tag{9}$$

Considering the high-temperature conditions, the relevant PA helps proton hopping even without water. That is why the PA-doped PBI membrane enhance the proton exchange properties under high temperatures.

It was also reported that protonated phosphonic acid electrodes remarkably improved the performance of high-temperature PEM fuel cells. A perfluorosulfonic acid proton can be transferred to the phosphonic acid to enhance the anhydrous proton conduction of fuel cell electrodes. For example, a protonated phosphonic acid PEM fuel cell exhibited a rated power density of 780 mW cm^{-2} at 160 °C, with minimal degradation during 2 500 h of operation and 700 thermal cycles from 40 to 160 °C under load [91].

The degradation and failure mechanisms of membranes must be discussed. Harsh conditions, including open-circuit/idling and dynamic loads, can cause severe membrane degradation. The commonest failure mechanisms of proton exchange membranes can be divided into two categories: chemical and mechanical degradation [92]. The open-circuit/idling is the main trigger for chemical degradation, which is usually caused by oxygen molecules infiltrating from the cathode to the anode side. The trace oxygen on the anode side can be reduced by Pt catalysts and form harmful HOO· and HO· free radicals. The attack by free radicals then likely destroys the fluorocarbon main chain in the PFSA membrane, directly affecting the mechanical strength and proton conductivity of the membrane, which leads to membrane degradation (Fig. 7a) [93]. According to this chemical degradation mechanism, wiping out or reducing free radicals is critical. The grafting of free radical scavengers and organic antioxidants can help polymer membranes obtain superior chemical stability and maintain proton conductivities [94, 95]. It has been reported that when using cerium oxide as a radical scavenging agent within membranes, the working lifespan is much longer than that of the reference membrane under accelerated durability test conditions [96–98].

Another reason for membrane failure is mechanical degradation [7]. The harsh condition of dynamic load readily leads to membrane mechanical degradation (Fig. 7b). In a dynamic load protocol, mechanical stress is generated inside the membrane and causes mechanical degradation [10]. Additionally, the volume change of the membrane is very sensitive to humidity. In the fuel cell startup process, the membrane absorbs water and expands, leading to expansion pressure [99]. To improve the mechanical stability under complex stress, the membrane is usually strengthened by using porous polytetrafluoroethylene (PTFE) fibers. PTFE-reinforced PEMs can be obtained by multicoating PFSA ionomers onto porous PTFE webs prior to solvent evaporation. The application of PTFE-reinforced thin PEMs in fuel cells not only significantly contributes to the improvement of cell performance by reducing the internal cell resistance, but also reduces the usage of PFSA ionomers. At present, Gore-selective® membranes are the most commonly used membranes in commercial applications.

In addition to the membrane, the ionomer is an important component toward building a proton transfer network. As mentioned in Sect. 2.1, the tested ORR activity is different between using RDE and MEA. One of the main factors may be that a larger number of ionomers are needed in the thick catalyst layers in MEA tests than in RDE. Ionomers play an essential role in proton transfer and distribution across the catalyst layer but usually block the active sites and porous structures (Fig. 8a). Therefore, the desired catalyst layer highly depends on the ionomers. Moreover, the catalyst layer and the membrane present different requirements in PEM fuel cells. Although both require low swelling and chemical and mechanical durability [68], the major distinction between ionomers and membranes is that ionomers need high gas permeability, while membranes need low gas permeability. Therefore, using different polymers for catalyst layers and membranes might be an alternative solution.

Several research groups have reported significant improvements in fuel cell performance without any remarkable adverse effects by using highly oxygen-permeable ionomers (HOPIs) in the catalyst layer (Fig. 8b). Jinnouchi et al. reported that a HOPI incorporating a ring-structured monomer significantly enhances both the interfacial oxygen permeation and ORR activity. This occurs because the high oxygen solubility allows high permeation and mitigates catalyst poisoning by one or two oxygen atom(s) of the terminal sulfonate group [100, 101].

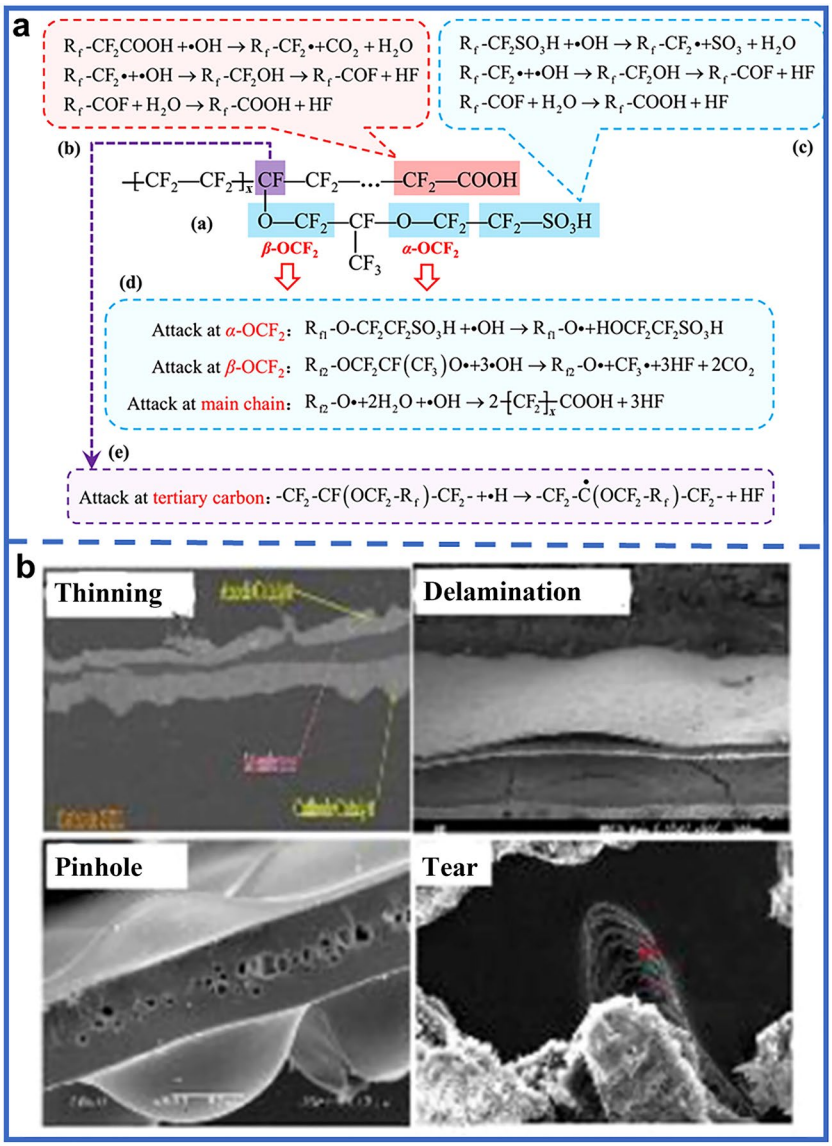

Fig. 7 **a** Chemical degradation mechanism of the PFSA membrane. Reprinted with permission from Ref. [22]. Copyright © 2020, Elsevier Ltd. **b** Various mechanical failures of the membrane. Reprinted with permission from Ref. [10]. Copyright © 2019, Elsevier Ltd

Major transport processes required for ORR are controlled by the thin ionomer film covering the Pt catalyst. After the interface between the ionomer and Pt has been formed, the sulfonic groups on the side chain of ionomers become oriented toward the catalyst surface, and an interface with phase separation forms. In contrast, the phase separation at the catalyst/ionomer interface is poor if the ionomer forms an interface with a weakly interacting substance such as carbon. Therefore, the interfacial structure depends on the surface properties of the catalyst (such as the concentration of Pt and the crystallinity of the carbon support), thus changing the physical properties of the ionomer, which in turn affects the water absorption, proton conductivity, and gas permeability at the interface [103, 104]. The use of short-chain ionomers with low equivalent weight and more sulfonic groups in the cathode catalyst layer (CCL) can improve the coverage and proton conductivity of ionomers compared with long-chain ionomers [104]. To result in ionomers being homogeneously distributed, the interaction between the carbon support and ionomer is of importance. The carbon support can be modified by introducing NH_x or N groups to obtain positive charges, thus promoting ionomer distribution on the carbon support [105]. Meanwhile, it is necessary to provide high IEC without inducing negative effects on the catalyst and to further provide high oxygen permeability [100, 103, 104, 106, 107]. Ideally, the ionomer should be evenly distributed in the catalyst layer to realize the most accessible active sites, the lowest oxygen transport resistance, and sufficient proton conductivity. The performance of PEM fuel cells can be effectively improved by optimizing the catalyst/ionomer interface during MEA manufacturing.

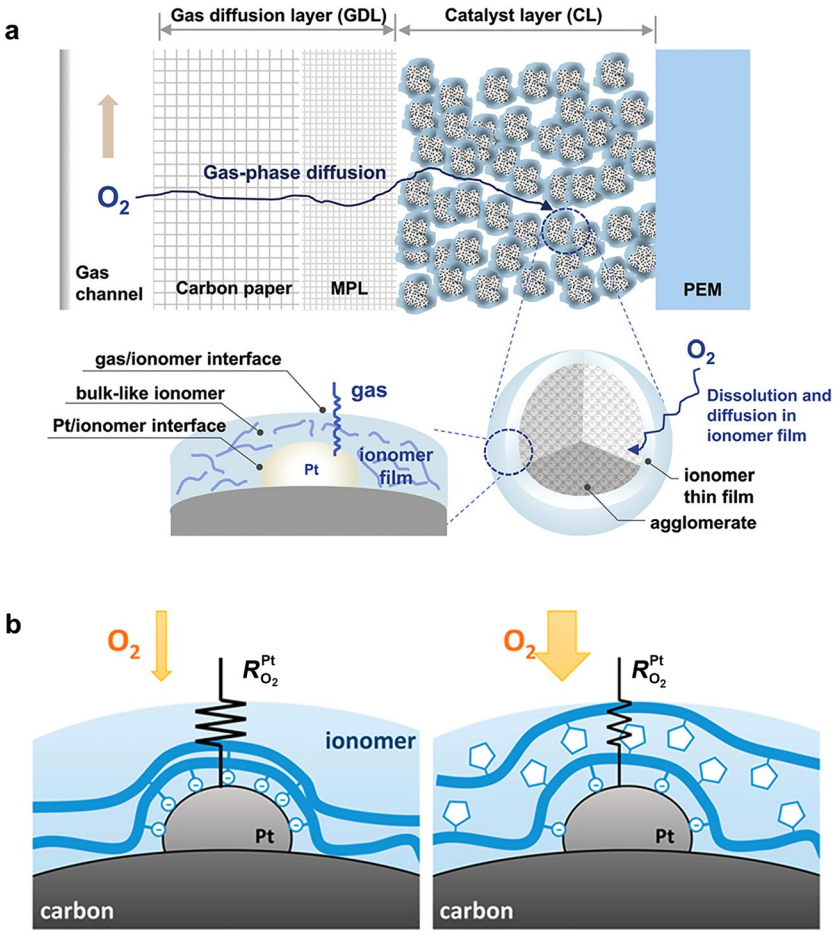

Fig. 8 **a** Schematic diagram of the oxygen diffusion pathways in PEMFCs. Reprinted with permission from Ref. [102]. Copyright © 2022, The Royal Society of Chemistry. **b** Schematic diagrams of the hypothesized ionomer structure at the Pt surface for conventional ionomers and high-oxygen-permeable ionomers. Reprinted with permission from Ref. [65]. Copyright © 2016, American Chemical Society

2.3 Gas Diffusion Layer (GDL)

GDL usually consists of a substrate layer (usually carbon cloth, carbon paper, and carbon felt, as shown in Fig. 9a–c) and a microporous layer (MPL). The MPL is coated on the hydrophobic treated substrate layer [108–110]. In MEAs, as shown in Fig. 1b, the MPL is in direct contact with the catalyst layer, and the substrate layer is in contact with the outside bipolar plate (BPP) [110].

Given the location of the GDL in the MEA, it is easy to understand the functions of the GDL, which provides stable mechanical support and corrosion resistance to protect the catalyst layer from damage and maintains good interfacial contact with the catalyst layer and BPP to ensure smooth flow of each transmission channel (e.g., electricity, heat, water) [108, 112–114]. During the operation of a fuel cell, electrons are efficiently conducted between the BPP and the catalyst layer via the GDL, and similarly, the heat generated by the catalyst layer is efficiently transferred to the BPP via the GDL. Therefore, the GDL mainly serves the important functions of conducting electricity and heat and transporting reaction gases [115, 116].

As shown in Fig. 1c, protons transport from the anode to the cathode along with the water flow. It is thus necessary to maintain sufficient water at the anode side to ensure efficient proton transport [117–119]. Accordingly, the GDL at the anode side requires a certain degree of hydrophilicity to ensure that there is enough water for the membrane and ionomer to conduct protons. However, according to Eq. 2, the cathode reaction produces a large amount of water (especially under heavy working conditions), some of which is transferred through the PEM to the anode, while the rest of which needs to be efficiently exhausted through the GDL to the flow fields [120]. Without proper exhaust, the water can cause a series of problems due to flooding at the cathode. The problem of water management on the cathode side is opposite to that on the anode side. Therefore, the GDL on the cathode needs to be more hydrophobic than that near the anode [121, 122]. GDLs at both sides need to possess a suitable pore size distribution, porosity, and pore structure to allow the liquid water in the CL to enter the GDL [123].

Combining these requirements, an ideal GDL should meet the following criteria: (1) sufficient mechanical stability (high compression ratios and high bending stiffness);

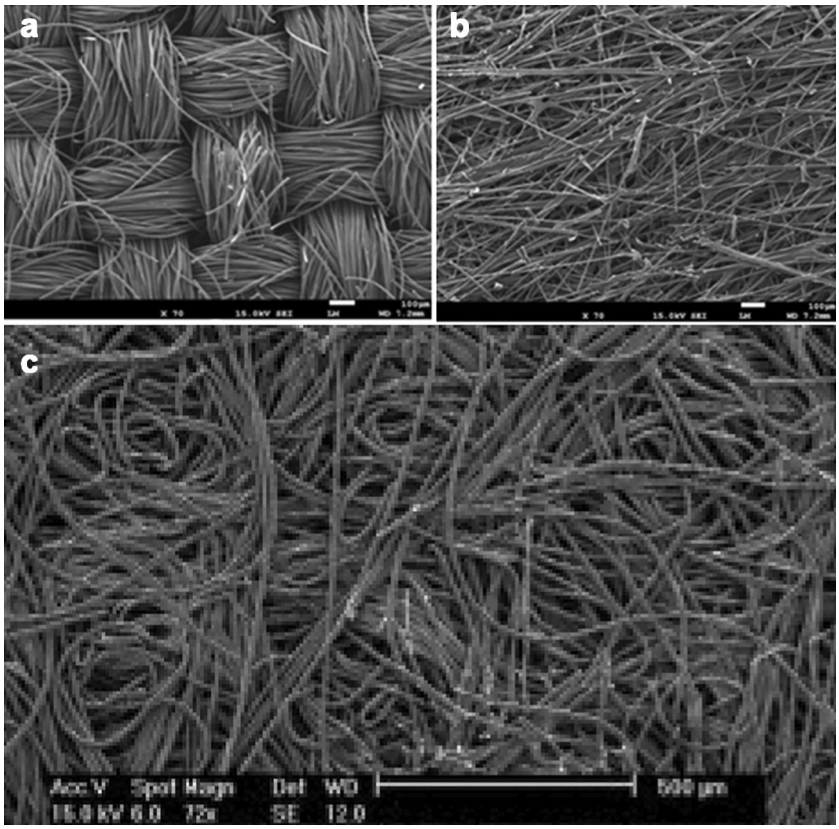

Fig. 9 SEM images of **a** carbon cloth, **b** carbon paper, and **c** carbon felt. Reprinted with permission from Ref. [111]. Copyright © 2022, Elsevier Ltd

(2) excellent chemical stability (surface stability and high corrosion resistance); (3) excellent electrical conductivity; (4) high thermal conductivity; (5) suitable pore size distribution, pore structure, and porosity; (6) excellent gas permeability; and (7) suitable hydrophilicity and hydrophobicity [108–110]. In the pursuit of optimum PEM fuel cell performance, it is essential to optimize the GDL [108, 109, 124, 125]. Current research advances in GDLs revolve around optimizing water management by enhancing MPLs and the structure of GDLs.

It has been widely accepted that optimizing MPLs is an efficient strategy to assist in water management [126]. MPL minimizes the contact resistance between the CL and GDL and is effective in limiting catalyst ink entry into the GDL and active material loss. Currently, optimization and improvement of MPLs revolve around (1) the thickness of MPLs [127–129], (2) the porosity and pore size distribution of MPLs [130–133], (3) hydrophobic or hydrophilic modifications of MPLs (Fig. 10a) [134–138], (4) MPLs with multiple hydrophilic and hydrophobic layers [139–143], and (5) modifications of MPL structures (Fig. 10b) (e.g., cracks and perforations as the liquid water pathway to the substrate layer, etc.) [144–149].

The hydrophobicity of GDL conventionally comes from the employment of hydrophobic agents. However, these agents cannot withstand high sintering temperatures. Therefore, most of the studies at present are focused on structural modifications of GDLs to enhance their water transfer

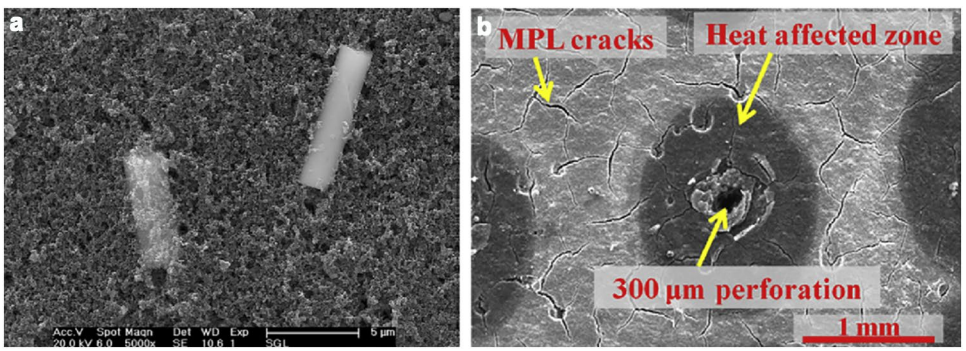

Fig. 10 **a** MPL with hydrophilic fibers (i.e., aluminosilicate fibers) to improve water removal by providing preferred water pathways. **b** SEM image of the MPL surface showing the heat-affected zones around holes generated by the laser when both the substrate and MPL are perforated. Reprinted with permission from Ref. [110]. Copyright © 2017, Elsevier Ltd

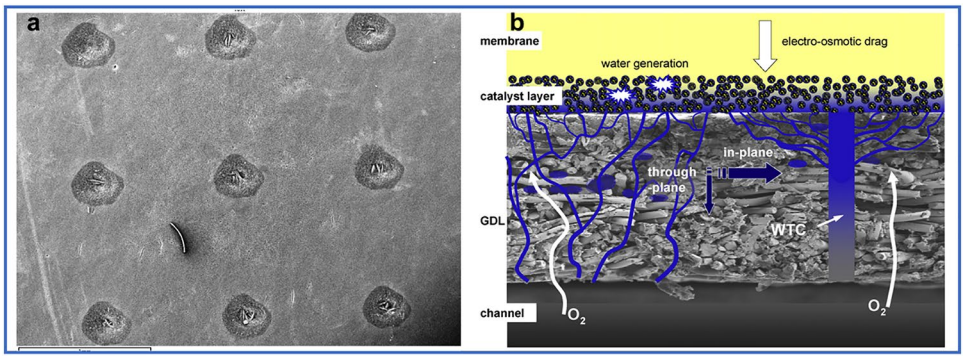

Fig. 11 **a** SEM image of a perforated GDL. Reprinted with permission from Ref. [151]. Copyright © 2013, The Electrochemical Society. **b** Schematic diagram of liquid water transport with and without a water transport channel. Reprinted with permission from Ref. [153]. Copyright © 2010, Elsevier B.V

Table 1 Physical/electrochemical characterizations needed to preliminarily screen ORR catalysts

Characteristic	Calculation or test method	Refs.
Electrochemical active area (A_{ECA}) ($m^2\ g_{Pt}^{-1}$)	$A_{ECA} = \frac{100 \times S}{0.21 V \times m_{Pt}}$	
Mass activity (λ_{MA}) at 0.90 V ($A\ mg_{Pt}^{-1}$)	$\frac{1}{j} = \frac{1}{j_k} + \frac{1}{j_{lc}} = \frac{1}{j_k} + \frac{1}{0.62nFAC_0^* D_0^{\frac{2}{3}} v^{-\frac{1}{6}} \omega^{\frac{1}{2}}}$	[159]
	$\lambda_{MA} = \frac{j_k}{m_{pt}}$	
Specific activity (λ_{SA}) at 0.90 V ($mA\ cm^{-2}$)	$\frac{1}{j} = \frac{1}{j_k} + \frac{1}{j_{lc}} = \frac{1}{j_k} + \frac{1}{0.62nFAC_0^* D_0^{2/3} v^{-1/6} \omega^{1/2}}$	[160]
	$\lambda_{SA} = \frac{j_k}{A_{ECA}}$	

S is the hydrogen desorption peak area; V is the scan rate; m_{Pt} is the mass of Pt; j, j_k, and j_{lc} are the measured, kinetic, and diffusion-limited current densities, respectively.

capacity, e.g., perforation (Fig. 11a) [109, 110]. Perforating the GDL can also be effective in optimizing the water management performance of the GDL. Most of the current research in this area has been carried out by microdrilling, electrodischarge machining (EDM), or laser perforation to create preferential water channels along diffusion channels in GDL structures [150–157]. Water flows out through the perforated water channels, while the gas moves through the diffusion channels (Fig. 11b). It has been shown that during EDM or laser perforation, the diffusion channels around the water channels gain some hydrophilic pores due to the degradation of the hydrophobic layer. This strategy improves the wettability of the GDL while enhancing liquid water removal, effectively improving water management performance [150, 152, 158].

2.4 Materials Screening Prior to MEA Manufacturing

All the abovementioned advanced materials serve better MEA manufacturing. Although the performance of each key material has been significantly improved, some of these are still far from being implemented in commercial applications because they cannot meet the preliminary requirements. In an established MEA manufacturing line, a large amount of characterization is initially required prior to integrating these new materials. The main properties that need to be characterized to screen for suitable materials are listed in Tables 1, 2, 3 and 4. Finally, the selected materials to be integrated

Table 2 Physical/electrochemical characterizations needed to preliminarily screen the membrane

Characteristic	Calculation or test method	Refs.
Proton conductivity (σ) ($S\ cm^{-1}$)	$\sigma = \frac{L}{RS}$	[161]
Water uptake (W) (%)	$W\%(RH) = (W_{RH} - \frac{W_{dry}}{W_{dry}}) \times 100$	[162]
Swelling rate (α_{SW}) (%)	$\alpha_{SW}(\%) = \frac{D_{wet} - D_{dry}}{D_{dry}} \times 100\%$	[163]
Rate of gas crossover ($cm^2\ s^{-1}$)	$D_i^{mem} = \frac{K_i^{mem}}{S_i^{mem}}$	[69]

L is the distance between the two electrodes in cm, R is the resistance value of the membrane and S is the cross-sectional area of the membrane in cm^2; D_{wet} and D_{dry} are the thicknesses of the wet and dry membranes, respectively; S_i^{mem} and K_i^{mem} represent the gas solubility in mol m^{-3} Pa^{-1} and the gas permeability coefficient in mol m^{-1} Pa^{-1} in membranes, respectively.

Table 3 Physical/electrochemical characterizations needed to preliminarily screen ionomers

Characteristic	Calculation or test method	Reference
IEC (mequiv g^{-1})	$IEC = \frac{\text{consumed NaOH(ml)} \times \text{molarity NaOH}}{\text{weight of dry membrane}}$	[161]
Trace metal element content ($\mu g\ g^{-1}$)	ICP−OES	

Table 4 Physical/electrochemical characterizations needed to preliminarily screen GDL

Characteristic	Calculation or test method	Reference
Pore structure	Capillary flow porosimetry $D = \frac{4\gamma\cos\theta}{P}$	[164]
In-plane electrical conductivity (Ω cm)	Four-probe method $\rho_{GDL} = CtR$	[164]
Through-plane electrical conductivity (Ω cm)	$R_{TP} = \frac{U_m}{I} \times A$	[116]
In-plane thermal conductivity coefficient (W m^{-1} K^{-1})	$k_{GDL,in} = \frac{L}{Wt}(\frac{1}{R} - \frac{1}{R_0})$	[164]
Effective diffusion coefficient (cm^2 s^{-1})	$D_i^{eff} = \frac{ft}{R_{GDL}}$	[164]
Surface wettability	Sessile drop technique	[164]
Mechanical properties	Tensile strength & compressibility	[164]

D is the pore diameter, γ is the surface tension of the working fluid, θ is the contact angle of the working fluid, P is the pressure difference between the nonreacting gas and working fluid; ρ_{GDL} is the bulk resistivity of the GDL sample, C is the geometry-dependent correction factor, t is the thickness of the GDL sample, R is the calculated resistance; R_{TP} is the through-plane resistance, U_m is the measured voltage drop, I is the constant current, A is the surface of the specimen; L is the length of the heat transfer pathway, W is the sample width; f is the geometry-dependent correction factor.

into an MEA require further testing and quality inspection, followed by large-scale manufacturing [2].

3 State-of-the-Art Membrane Electrode Assembly Manufacturing Processes

The MEA fabrication process generally includes ink dispersing, electrode coating, electrode drying, slitting and cutting, component assembly, and pressing (Fig. 12a–f). In the following sections, we will discuss the progress of each step toward complete MEA manufacturing by dividing them into three parts, i.e., electrode processing, cell assembly, and quality assurance.

3.1 Electrode Processing

3.1.1 Ink Dispersion Step

The goals of the electrode ink mixing step are to break up catalyst agglomerates and maximize the affinity between catalyst and ionomer, i.e., dispersion degrees. The quality of catalyst ink dispersion plays a major role in determining the final electrode structure and in turn influences the performance and durability of the PEM fuel cell. Catalyst ink

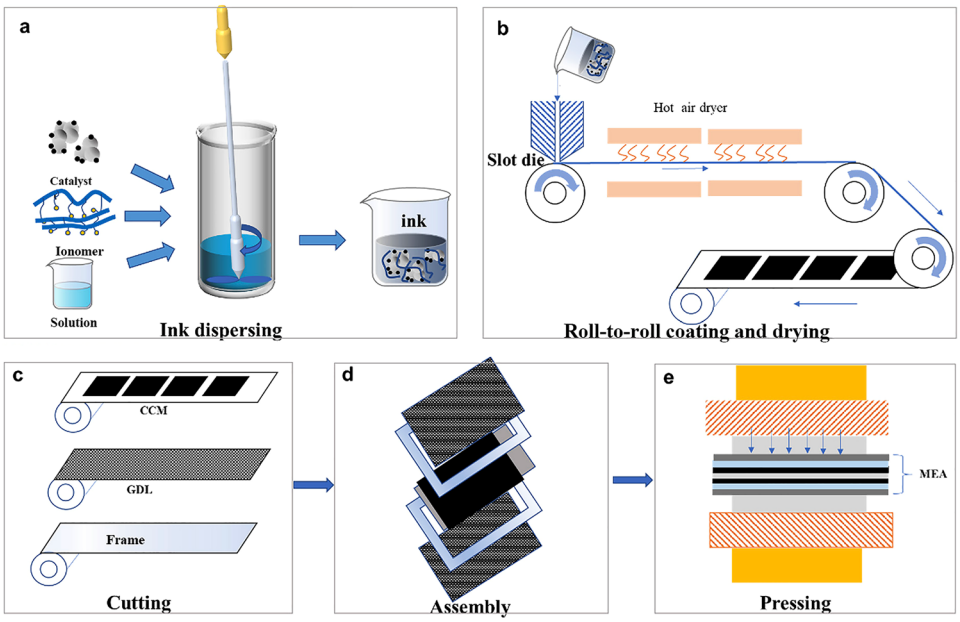

Fig. 12 **a–e** General MEA fabrication process, including ink dispersing, coating, drying, cutting, assembly, and pressing

usually contains solvent, ionomer (e.g., Nafion), and catalyst powder. To achieve high electrode performance in terms of activity and/or durability, understanding and optimization of the ink formula are important. The catalyst/ionomer interface depends on the interaction between the catalyst and ionomer, as well as the dispersion of the catalyst/ionomer in the solvents. Many methods/techniques have been proposed for electrode ink preparation, including ultrasonic dispersion [165], sonication [166], ball milling dispersion [167], mechanical shear dispersion, and high-pressure homogenization dispersion (Fig. 13a–c) [168].

Extended molecule chains of ionomers possess a hydrodynamic diameter between 20 and 30 nm. In primary aggregation, the ionomer aggregate diameter is approximately 300 nm due to the hydrophobic interaction of the fluorocarbon backbone. In secondary aggregation, ionomer aggregates with a diameter above 1 000 nm form via electrostatic interactions of side-chain ion pairs [170]. In catalyst ink, however, ionomer aggregation is undesired. The solvent for the ionomer solution affects the aggregate size. The aggregation size of short side-chain ionomers can be controlled by increasing the dipropylene glycol (DPG) content (the solvent) because the hydrophobic backbone main chain of short side chain ionomers becomes more mobile due to their high solvating power. Reasonably, the decreased ionomer aggregation leads to a more homogeneous ionomer distribution in the catalyst layer, which can facilitate proton transfer at low relative humidity (RH) conditions [171]. The application of different solvents in ionomers also shows a significant effect on MEA durability. It was specifically shown that non-aqueous dispersion solvents are more beneficial than aqueous solvents [172]. For the requirements for long lifetime applications, such as heavy-duty fuel cell vehicles (where the US DOE targets 25 000 and 30 000 h in 2025 and 2030, respectively), this effect should particularly be considered. Therefore, the content of alcohol as a solvent in the ionomer solution can be adequately increased to enhance the service life of final MEAs.

A solvent is also needed when preparing the catalyst ink, in addition to the ionomer solution. Ink formulation is a critical factor for the formation of catalyst layers. It should be noted that the solvent used for catalyst ink preparation does not need to be the same as the solvent for ionomer solution. The size distribution of aggregates (containing both

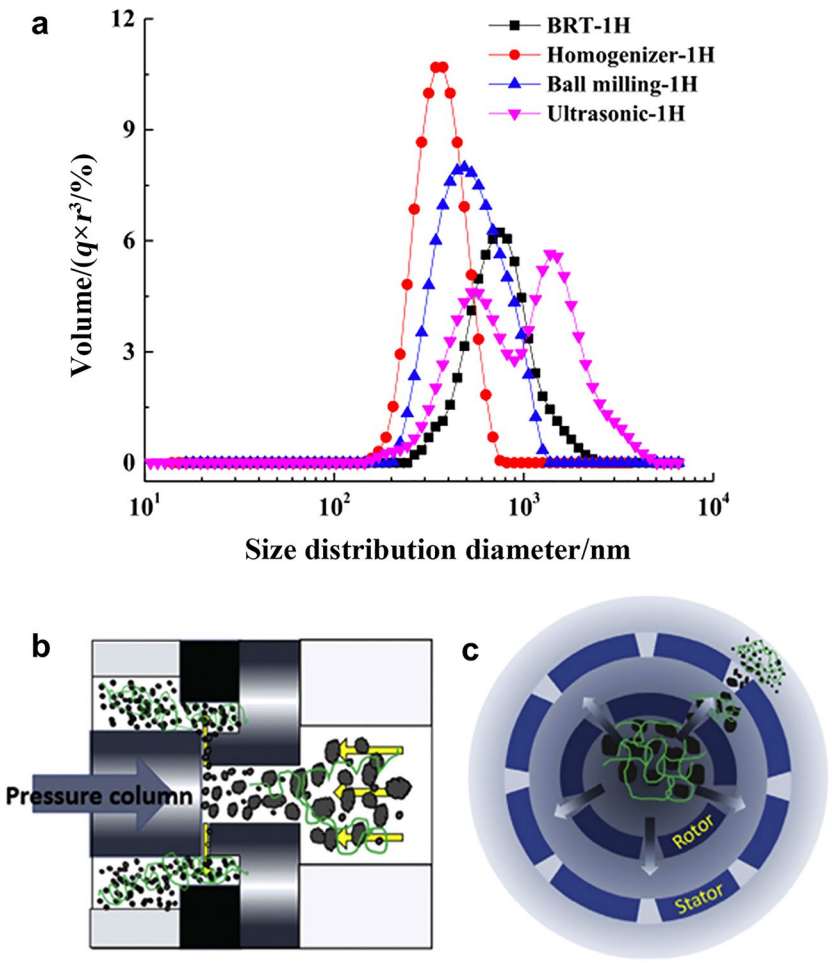

Fig. 13 **a** Hydrodynamic diameter distribution of clusters in slurry prepared by different dispersion equipment. Illustrations of the **b** high-pressure homogenizer method and **c** high-shear emulsifier method. Reprinted with permission from Ref. [169]. Copyright © 2022, Elsevier Ltd

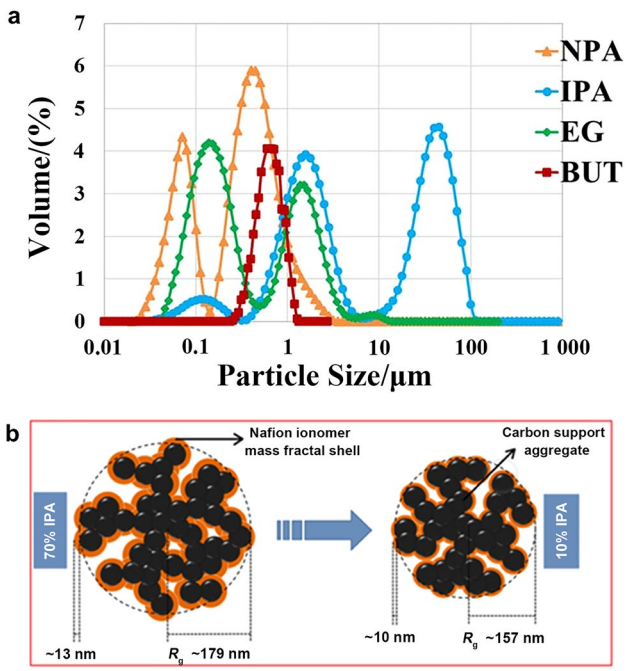

Fig. 14 **a** Pt/C agglomerate size distribution of catalyst inks dispersed in different solvents measured by laser diffraction. Reprinted with permission from Ref. [172]. Copyright © 2021, Electrochemical Society, Inc. **b** Schematic illustration of the effects of reducing the alcohol content in isopropyl alcohol/water on the colloidal structure of the prepared fuel cell catalyst ink. Reprinted with permission from Ref. [179]. Copyright © 2019, American Chemical Society

the ionomer and catalyst), as well as the stability and viscosity in catalyst ink, significantly depends on the quality of the dispersion solvent (Fig. 14a). The solvent in the catalyst ink tailors the micro/nanostructure of the catalyst/ionomer interfaces [173]. First, the dielectric constant of the solvent affects the catalyst–ionomer aggregation size: when excessively high or low, the dielectric constant leads to significant ink agglomeration. A solvent with a moderate dielectric constant would be helpful in improving the ink stability [174, 175]. In addition, the solvent composition should be considered. For example, solvents with high boiling points usually form larger catalyst–ionomer aggregates in the final catalyst layer, resulting in more secondary pores and lower mass transport resistance [176, 177]. However, high boiling point solvents require higher temperatures for drying, presenting higher toxicity and leading to severe swelling of the PEM [178]. Traditional ink solvents are used as organic solvents. Recently, to decrease the cost and mitigate the environmental risks associated with organic solvents, the water-rich catalyst ink strategy has been receiving rapidly growing interest (Fig. 14b) [179].

In addition to the solvent, the ratio of ionomer to carbon, namely, the *I*/*C* ratio, is also crucial in catalyst layer structure optimization. The ionomer plays an important role in dispersing ink—homogeneous ink cannot form without the assistance of the ionomer [167]. It was reported that the catalyst can absorb more ionomers in a high *I*/*C* ratio, thus increasing the fracture toughness of catalyst layers and reducing crack width [180]. However, a high *I*/*C* ratio may result in negative effects. In the catalyst layer, inhomogeneous ionomers cover active sites, decrease the available active site density, and increase the local oxygen transport resistance, thus leading to ORR activity loss. Therefore, neither a high nor low *I*/*C* ratio is desired. The MEA with a moderate ionomer content of ~ 26 wt.% (wt.% means the weight percentage) shows the highest performance in terms of electrokinetic parameters, such as ECSA, suggesting balanced electronic and ionic percolation within the catalyst layer [181]. Notably, the ionomer requirement depends on the Pt loading. It has been found that the optimal ionomer content increases as the Pt loading decreases [182].

The properties of the ionomer itself are also aligned with the catalyst layer quality. Usually, ionomers with lower equivalent weights (EWs) possess higher proton conductivity [183] but are sensitive to water. In this regard, using a low EW ionomer readily leads to a swelling phenomenon. For example, in the representative Pt–Co alloying catalyst ink, applying a low EW ionomer causes more loss of Co and of lattice contraction compared to Nafion ionomer [184]. Nevertheless, the choice of ionomer depends on the catalyst type because the dispersion of catalyst ink depends on not only the solvent and ionomer but also the interaction of ionomer and carbon particles in the ink [185].

To reduce local mass transport resistance through the platinum–ionomer interface, the coverage of the ionomer over the catalyst needs to be uniform. One approach for achieving a homogenous distribution is by modifying the carbon support with N functional groups [186]. In this regard, the Coulombic interaction between the ionomer and N groups on the carbon support helps homogeneous ionomer distribution and improves reproducibility during the ink manufacturing process [187]. Moreover, a high-surface-area carbon support demonstrates a higher ink viscosity due to both a higher internal porosity and a more agglomerated structure that increases the effective particle volume fraction [176]. Therefore, to obtain a higher ink viscosity coating, applying a high-surface-area carbon support catalyst is the desired technique.

Temperature is a key parameter in the fabrication of catalyst inks, which may be overlooked during the preparation of catalyst inks. It is preferred to prepare the catalyst ink in an ice bath due to the shear-thinning behavior at elevated temperatures [188]. The catalyst ink must be mixed for a sufficiently long period to obtain good and stable cell performance. Once the catalyst ink forms, the aggregation evolution should be considered as it depends on storage time and conditions. As shown in Fig. 15a–c, the state of the catalyst ink remarkably changes within 24 h of storage [189].

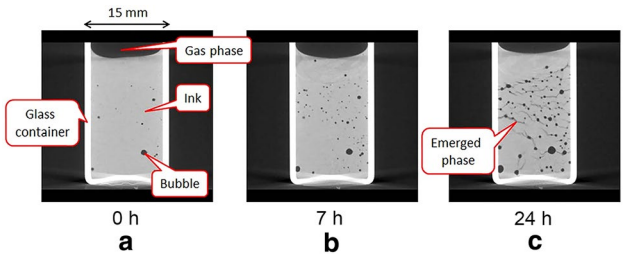

Fig. 15 **a–c** Slice images of the interior of a catalyst ink sample show the state of the ink changing markedly over time. Reprinted with permission from Ref. [190]. Copyright © 2018, The Electrochemical Society

Before proceeding to the coating step, the catalyst ink needs to pass a comprehensive evaluation. Conventional visual inspection of the catalyst ink is insufficient due to the difficulties in tracking variations in the catalyst ink over time. Therefore, a comprehensive evaluation including the aggregation scale, particle size distribution, zeta potential (ξ), and rheological properties such as viscosity, surface tension, and contact angle is necessary [180]. Then, the large agglomerates and air bubbles in the catalyst ink should be removed to minimize spots in the coating films.

3.1.2 Coating Step

The catalyst layers for MEA are typically fabricated through two methods: catalyst-coated substrates (CCS) [191] and catalyst-coated membranes (CCM) [191]. In the case of CCS, the as-prepared catalyst inks are coated on the GDLs to form electrodes (anodes and cathodes, to be specific), which are then sandwiched with the membrane. The CCS method is usually employed in laboratory investigations due to its easy operation and control. However, for industrial production, CCS offers low efficiency. Alternatively, the CCM method is widely used in the manufacturing line, which directly coats anode and/or cathode catalyst inks onto both or one side of membranes prior to pressing with GDLs. It has proven that the MEAs prepared by the CCM method not only offer high catalyst utilization but also show a smaller contact resistance and charge-transfer resistance, which results in the fuel cells demonstrating promising power output [192]. If the catalyst ink is coated on one side of the membrane, a decal transfer process is required that transfers the catalyst layer coated on a substrate (usually PFTE) to the membrane coated with the catalyst ink on another side, typically in a hot-pressing transfer step. Such a method is often used to prevent solvents from swelling the PEM [193]. However, compared to the direct coating process on both sides of the membrane, the decal transfer process cost is higher. Assuming a production volume of 500 000 per year for light-duty vehicle stacks, the total cost of decal substrate material and transfer processes is approximately 1.67 times the electrode coating process [193].

The coating method includes screen printing, inkjet printing, spray coating (Fig. 16a), doctor blade coating/knife coating (Fig. 16b), and slot-die-coating (Fig. 16c) [194–200]. To date, the most widely used electrode-coating instrument for reliable upscaling is the slot-die coater [201]. The slot-die coating process is a continuous process that benefits industrial production. Importantly, the electrodes produced by slot-die coating have shown superior film homogeneity. By applying the slot die coating process, appropriate operating parameters, such as the coating speed, flow rate, vacuum pressure, coating gap, liquid viscosity and surface tension can be adjusted and controlled properly [202]. The uniformity of the wet layer applied by slot-die deposition, for instance, is affected by process parameters such as substrate speed, vacuum pressure applied at the upstream meniscus, the gap between the slot die lips and substrate, ink rheology, and other ink and substrate properties (Fig. 17a, b) [202].

At present, the most advanced technique for meeting production volume requirements with continuous CCM production is the roll-to-roll (R2R) coating process. A schematic illustration of R2R coating technology is shown in Fig. 17c, d. Its advantages of high throughput and environmental friendliness are expected at various industrial sites [204]. The R2R coating technique can be adapted to manufacturing in accordance with target specifications, such as the coated layer thickness, rate and dimension of the coating product, and width of the coated film [203]. The catalyst coating quality is determined by balancing the stability of the catalyst ink and the coating conditions [205].

During the coating process, cracks and voids inevitably appear. Cracks and interfacial voids present both advantages and disadvantages [207]. On the one hand, cracks and voids

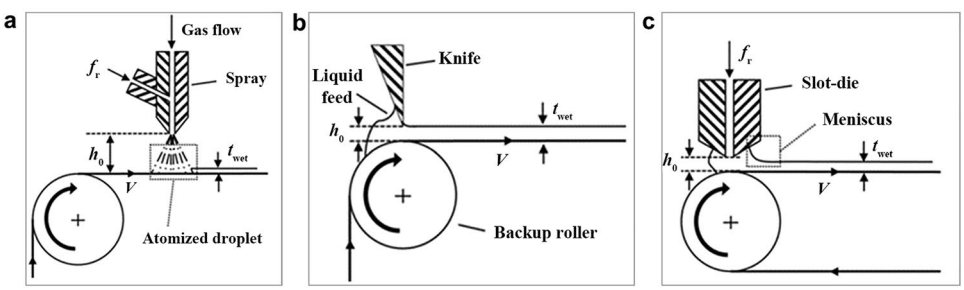

Fig. 16 **a–c** Spray coating, knife-over-edge coating, slot-die coating. Reprinted with permission from Ref. [203]. Copyright © 2016, Springer Nature

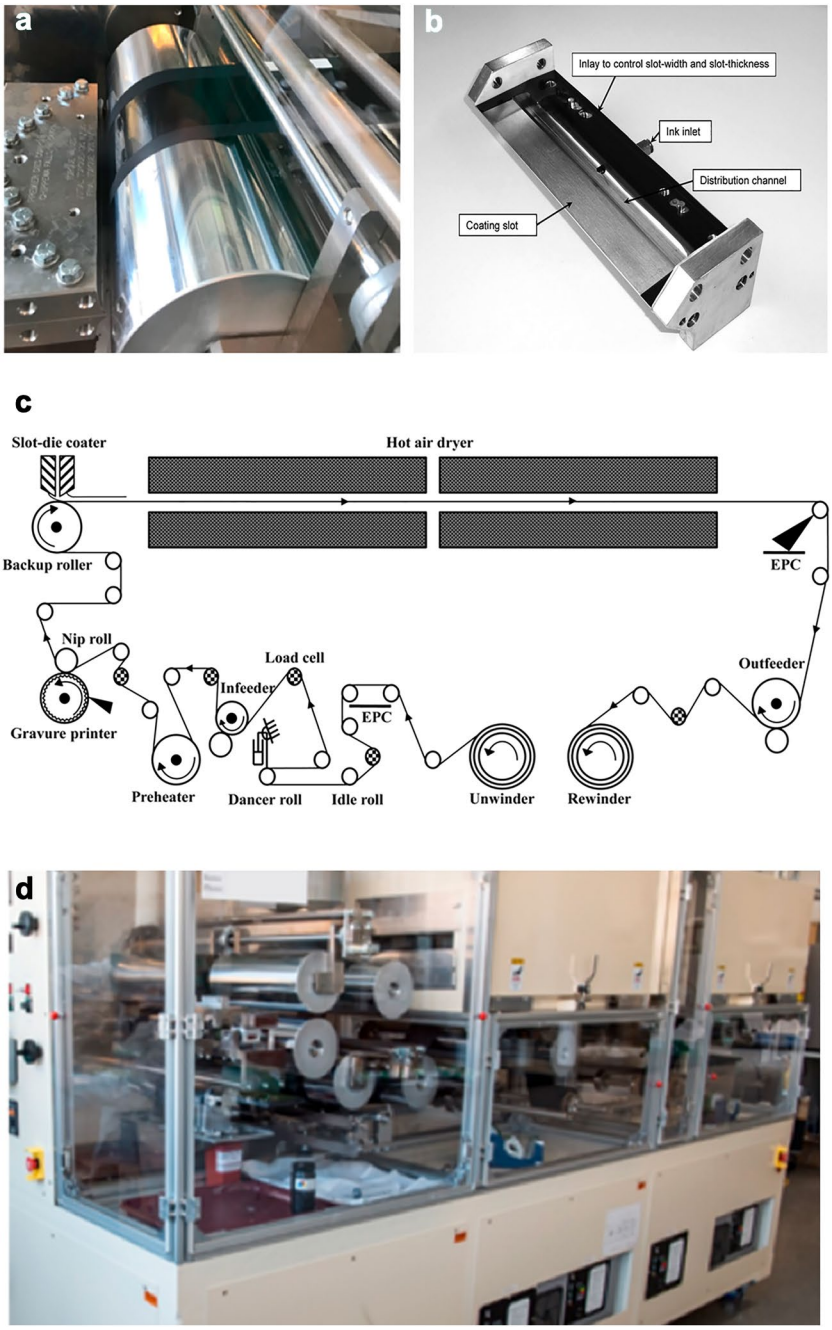

Fig. 17 **a** Photographs of the slot die coating using R2R. Reprinted with permission from Ref. [193]. Copyright © 2021, Elsevier B.V. **b** A slot-die is used for testing the distribution along its width and for coating with carbon ink, and a flat plate is used to close the slot-die. Reprinted with permission from Ref. [206]. Copyright © 2013, ASME **c** Configuration of a general R2R printing and coating system. Reprinted with permission from Ref. [203]. Copyright © 2016, The KSPE and Springer. **d** Photographs of the roll-to-roll coating station. Reprinted with permission from Ref. [193]. Copyright © 2021, Elsevier B.V

possibly deteriorate cell performance due to less electrical contact in the MEAs, reducing the MEA lifespan. On the other hand, cracks can enhance liquid and gas transport in the MEA. Therefore, it is important to balance crack and void formation to ensure high performance and durability under the operating conditions of PEM fuel cells [208]. Cracks and voids can be controlled by optimizing the ink formula. The addition of a high boiling point solvent [propylene glycol (PG)] to the catalyst ink can suppress crack formation [194]. This occurs because the solvent with a high boiling point is retained during drying, thus inhibiting the agglomeration of Pt/C particles and reducing the generation of cracks.

3.1.3 Drying Step

Drying is an indispensable step in the production of catalyst layers. The goal of the electrode drying step is to remove the solvent and create an electrode with uniform morphology, structure, and properties (Fig. 18a). During drying, the solvent molecules near the surface are vaporized first. Therefore, drying is a key process that controls the porous

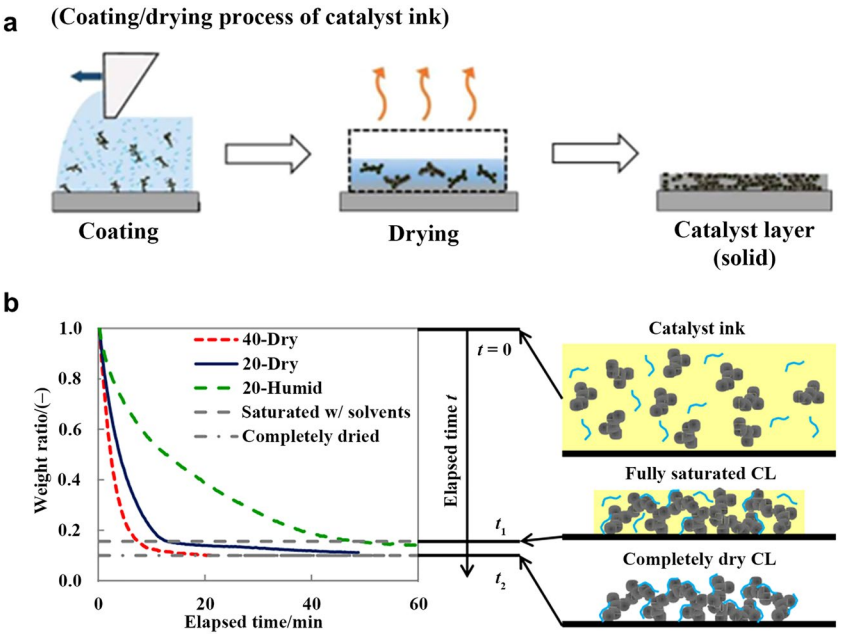

Fig. 18 **a** Fabrication process steps of the catalyst layer. Reprinted with permission from Ref. [211]. Copyright © 2018, The Electrochemical Society. **b** Weight variation of the catalyst ink at constant temperature and humidity and schematic diagrams of the state of the catalyst ink at representative times. The samples were dried at 40 ℃ and 0% RH (40-Dry), 20 ℃ and 0% RH (20-Dry), and 20 ℃ and 80% RH (20-Humid). Reprinted with permission from Ref. [210]. Copyright © 2016, Elsevier Ltd

structure because it affects the rate of solvent evaporation and void reduction. Meanwhile, the drying step is helpful in removing solvents in catalyst layers and enhancing cell performance [209]. Various physical phenomena can occur during drying, such as binder migration, membrane shrinkage, catalyst layer cracking, and sedimentation [210]. Accordingly, the drying temperature, drying rates, and drying humidity should be well controlled during this drying step (Fig. 18b).

The pore size distribution and specific pore volume in the catalyst layer can be modified by controlling the drying conditions. For example, raising the temperature during the drying step can facilitate the evaporation of the solvent in catalyst ink and induce a large pore volume, especially in terms of the secondary pore [212]. Meanwhile, when a thick liquid film catalyst layer is coated, its high evaporation rate leads to an enrichment of ionomer at the top surface of the dried layer [213]. In addition, the drying rate has little effect on the pore size formation but shows effects on the porosity [210]. We emphasize that material properties must be considered in parallel with altered drying conditions.

Common drying methods include vacuum drying, oven drying, and freeze drying. To reduce Pt loading, the thickness of the catalyst layer is currently very thin. For such a low-Pt-loading catalyst layer, one bottleneck is its high gas transport resistance. Therefore, it is necessary to consider the pore distribution to facilitate mass transport in the catalyst layer. Recently, it was found that freeze-drying offers advantages over common drying technology. Freeze-drying, commonly known as lyophilization, comprises the removal of the solvent directly from the solid phase to the vapor phase through sublimation, which results in an increase in porosity compared to other drying methods. This not only increases porosity but also forms a broader distribution of pores from the microscale up to the macroscale, thus improving Pt utilization [214, 215]. As shown in Fig. 19, after freeze-drying, the porosity of the catalytic layer is higher than that by using other drying methods. It was also found that freeze drying is more conducive to uniform distribution of ionomers in the catalyst layer [216].

To ensure the quality of the drying step, appropriate methods are needed to monitor the drying process and characterize the resulting catalyst layer. Contrast-variation

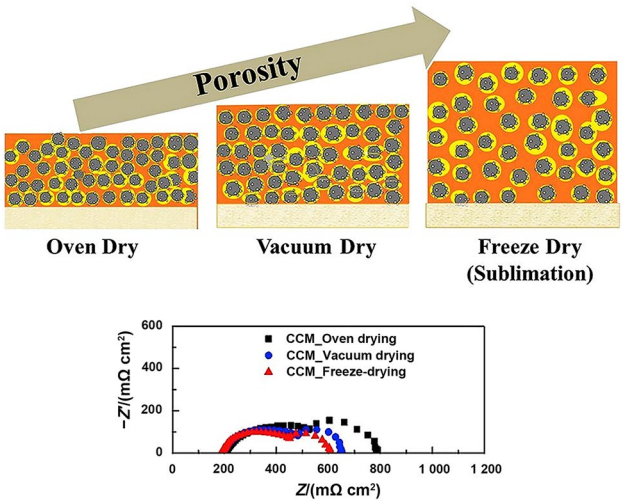

Fig. 19 Freeze-drying greatly increases the porosity of the catalyst layer, Nyquist plot for the CCMs at 500 mA cm^{-2} current density. Reprinted with permission from Ref. [214]. Copyright © 2019, Elsevier B.V

small-angle neutron scattering has been used to precisely measure the thickness of the catalyst layer. In addition, this method can elucidate the structural change of ionomers and carbon agglomerates during the drying process. For example, the size of the carbon agglomerates was observed to decrease along with solvent evaporation, while the thickness of the ionomer shell decreases as well during the drying process [217]. Pt/C catalysts generate aggregates during the drying process until the catalyst layer is completely dried [211]. ^{1}H NMR was also used to determine whether the catalyst layer was completely dried. The microporous structural changes of the catalyst layer could be detected by laser microscopy using ultrasmall angle X-ray scattering measurements and grazing-incidence X-ray scattering [194]. The drying rate is usually determined under atmospheric SEM collocation weight measurements [210].

Despite the effectiveness of the state-of-the-art electrode-manufacturing technology, undesired defects in the electrode cannot be completely avoided. These defects include cracks, spots, and coating irregularities [218, 219]. To assure the quality of the produced catalyst layer, accurate and timely on-site detection is essential. In-line quality control diagnostics for R2R manufacturing techniques plays a key role in the commercialization of PEM fuel cells. Infrared (IR) thermography has been widely utilized in fuel cell research as a nondestructive diagnostic tool for in-line quality inspection (Fig. 20a), which also works for the characterization of membrane pinholes [196, 218]. X-ray fluorescence spectroscopy measures the Pt loading of the catalyst layer [193]. Recent advances in the grazing-incidence small-angle X-ray scattering (GISAXS) computed tomography technique are emerging to efficiently characterize in situ CL and investigate the nanostructure of the catalyst layer during the ink drying process (Fig. 20b) [211]. Moreover, ex situ catalyst layer analysis is also necessary, such as through SEM and laser microscopy observation. Nitrogen-sorption porosimetry is also widely used for studying the morphology of micropores [220].

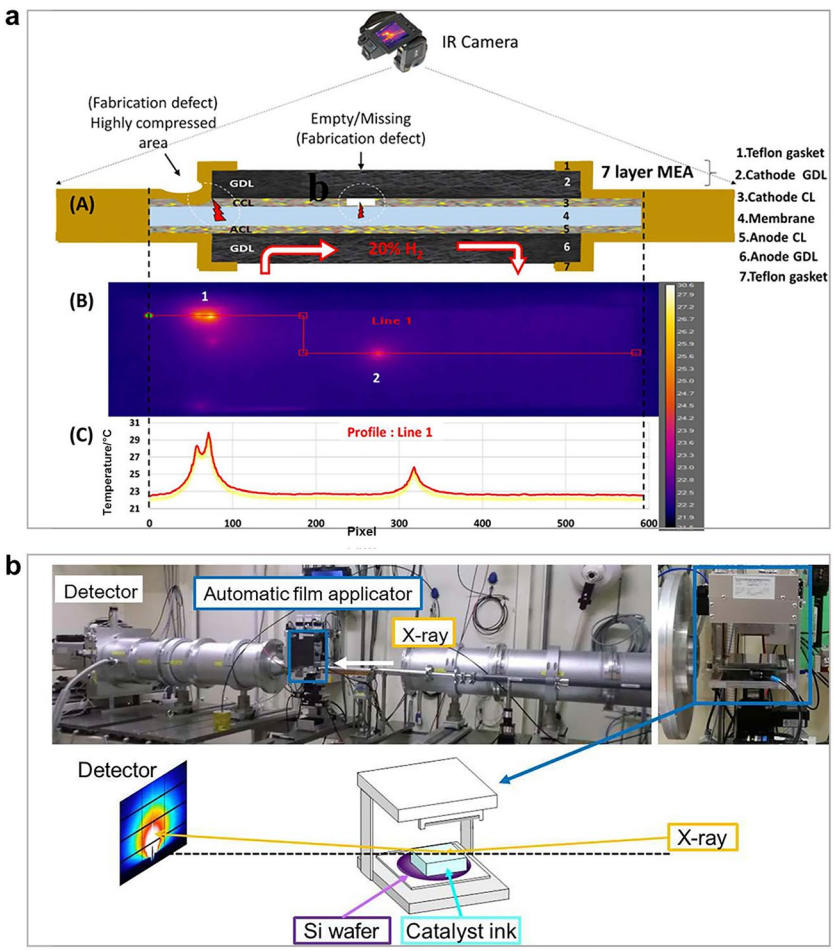

Fig. 20 **a** IR thermography to examine the cathode side of an MEA. Reprinted with permission from Ref. [196]. Copyright © 2018, John Wiley & Sons, Ltd. **b** After coating, an X-ray with a wavelength of 0.100 nm was irradiated on the catalyst ink film at an incident angle of 0.12°, and the scattering patterns were recorded at 1-s intervals on a PILATUS3X 2 M detector located at a distance of 3.5 m from the film. Reprinted with permission from Ref. [211]. Copyright © 2018, The Electrochemical Society

3.2 Cell Assembly

Eligible CCM products were obtained after electrode processing. They are then transferred to another line for MEA assembly.

3.2.1 Slitting and Cutting Step

The produced CCM products are provided in large rolls that need slitting and cutting to meet application requirements in terms of electrode shape and size. The slitting and cutting step is usually carried out by punch cutting or laser cutting. Accordingly, edge quality is an important factor. For a real-world production line, the cutting die must be monitored regularly during continuous production.

3.2.2 Assembly Step

The fabricated MEAs in the production line can usually be divided into five-in-one and seven-in-one configurations. The five-in-one structure signifies that both sides of CCM (2 catalyst layers and 1 proton exchange membrane) are attached to two frames, which offer support and sealing. Therefore, the match between CCM and frames significantly determines the sealing property. Usually, vacuum detection is needed to evaluate whether the sealing performance meets requirements. In addition, a seven-in-one structure refers to seven layers, including the five-in-one integration with two attached GDLs. The role of the GDL is discussed in Sect. 2.4. The assembly process is cumbersome and requires high alignment accuracy, so the yield is relatively low, suggesting that more precise and efficient industrial quality control is required.

3.2.3 Pressing Step

A pressing step may be needed to enhance the contact among each layer. At present, hot-pressing is a common technique. It has been found that to achieve the maximum performance of MEAs, hot-pressing conditions are crucial and should be optimized [221, 222]. It is logical that high pressing pressure provides better electrical contact between the cell components and reduces the ohmic loss. However, excessively high compression decreases the porosity in the GDL and leads to high mass transport resistance for reactants and products, as well as liquid water. Excessive pressure can also cause a breakup of GDL fibers and deteriorate the hydrophobicity, resulting in failures in water management [223, 224]. For example, it was reported that increasing the applied pressure led to high internal MEA resistance, which was attributed to the physical confinement of the Nafion membrane and thus limited water uptake in a fuel cell [225]. In addition to the pressure, the pressing time and temperature also present a significant influence on the cell performance (Fig. 21a, b) [226].

Overall, optimizing the pressing parameters requires comprehensive consideration of the materials, such as the membrane, frame, GDL, and temperature tolerance. To improve production efficiency, advanced strategies such as the self-assembled approach [228] and cold-pressing [229] have also been proposed to replace conventional hot-pressing. However, these approaches are not yet sufficiently mature.

3.2.4 Automatic Membrane Electrode Assembly Manufacturing

Based on the broad application prospects of fuel cells, industrialized mass production of membrane electrode assemblies (MEAs) is anticipated. Industrial production usually enables high efficiency and low cost, as is the case for the fuel cell industry. A manufacturing rate of several MEAs per second is thus required [230]. Toward high efficiency, automation is an inevitable approach (Fig. 22a). Automation can not only save labor costs but also be beneficial to improving precision control, therefore increasing product quality and improving yield. Taking the standard

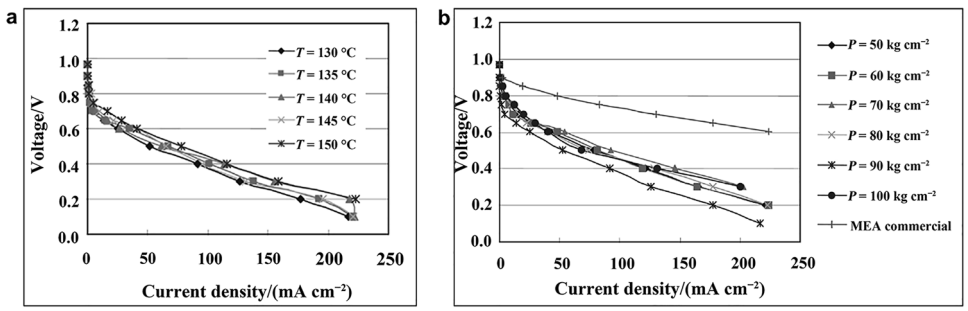

Fig. 21 **a** Polarization curve of MEA fabrication at different temperatures with a pressure of 100 kg cm^{-2} and a compression time of 1 min. **b** Polarization curve of the fabricated MEA at different pressures with a temperature of 150 °C and a compression time of 1 min. Reprinted with permission from Ref. [227]. Copyright © 2006, Korean J. Chem. Eng.

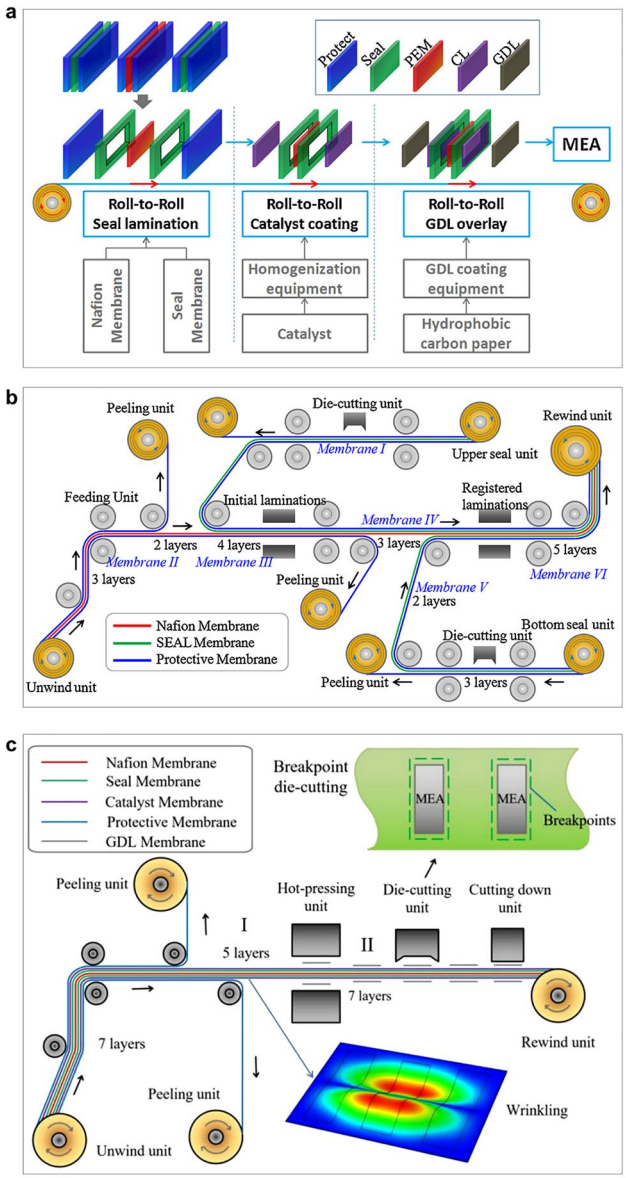

Fig. 22 **a** Complete MEA production line of fuel cells based on the R2R manufacturing system. Reprinted with permission from Ref. [231]. Copyright © 2016, Elsevier Ltd. **b** Equipment contains functions such as die cutting, waste film peeling, and multiple laminations (initial and registered laminations), which are integrated by the R2R system. The seal lamination equipment halves the protective film of Nafion, peels the cut scrap of the seal membrane off, and then, cold compresses the seal-Nafion seal to form a compound membrane. Reprinted with permission from Ref. [231]. Copyright © 2016, Elsevier Ltd. **c** GDL continuous overlaying system adopts R2R stack and lamination techniques. Reprinted with permission from Ref. [232]. Copyright © 2020, IMechE

seven-in-one MEA as an example, seven layers, including two GDLs, PEM, anode and cathode catalyst layers, and two seal frames, must be cut to the same size and aligned precisely. If a manual line is used, efficiency is low and product quality crucially cannot be guaranteed. Hence, there is significant interest in continually improving PEM cell reliability and manufacturing efficiency while reducing manufacturing costs. It is urgent to improve production efficiency through intelligent automation [231].

At present, R2R equipment is widely used in the catalyst ink coating step (the middle "Roll-to-Roll Catalyst coating" in Fig. 22a). However, for the former "seal lamination" and subsequent "GDL overlay" processes, the R2R technique has not yet been widely used. Figure 22b [231] and Fig. 22c [232] illustrate the R2R design for "seal lamination" and "GDL overlay", respectively.

3.3 Quality Assurance

The quality of produced MEAs is critical. In each step of MEA manufacturing, as discussed above, we have presented widely used approaches to perform in-line inspection, which can efficiently provide feedback to the MEA manufacturing line. Usually, both statistical process control techniques and process control strategies are needed, where statistical process control is used to determine the likelihood of defect-free products based on admissible error bands for process parameters, to trigger the process control strategy and correct the line as needed. If these two measures can be suitably combined, additional postproduction quality control steps may be eliminated [233].

As another important aspect of quality assurance, the close connection and, in particular, tight feedback between MEA manufacturing, suppliers and customers is important (Fig. 23). The MEA manufacturer can assure quality when delivering products based on specific/standard testing protocols. However, customers can require much more complicated working conditions that may not be captured by the existing specific/standard testing protocols. Therefore, timely feedback from customers supplies critical information to the MEA manufacturer. Furthermore, to meet the requirements of the customers, the materials provided by suppliers may also need further improvement. Over 99.9% of failure-free stacks at the beginning of the working lifetime are needed to be output from MEA manufacturing. This indicates less than one faulty MEA in 30 000 products [230].

4 Discussion of Material and MEA Manufacturing Processing Constraints

In the above sections, we have presented the most recent progress of key materials for MEAs and the manufacturing process of MEAs. However, current materials and manufacturing techniques still have their own limitations and constraints.

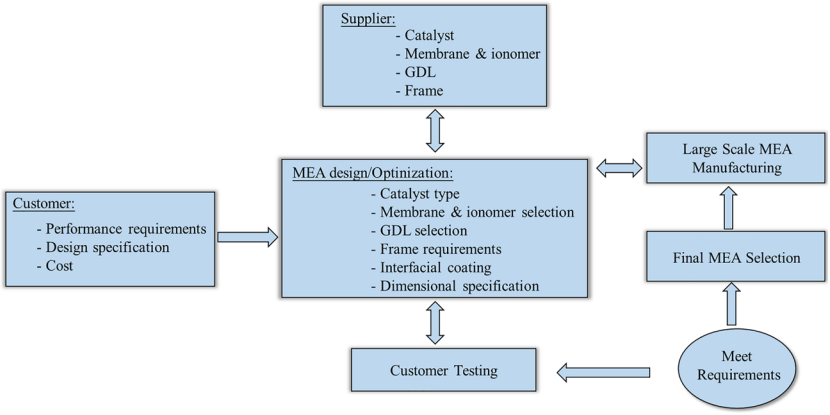

Fig. 23 Quality control flowchart for selecting a proper MEA. Redrawn with permission from Ref. [234]. Copyright © 2003, The Electrochemical Society

4.1 Material Constraints

Pt and its alloys remain the most applicable catalysts for PEM fuel cells. Since the cathode occupies most of the Pt usage, the majority of efforts have focused on ORR catalysts for PEM fuel cells [235–237]. To meet cost requirements, the loading of Pt needs to be further decreased. However, once Pt loading is decreased, the number of available active sites is also decreased, thus leading to severe performance loss [238, 239]. The barrier caused by low Pt loading has not been completely addressed. On the other hand, PGM-free catalysts, represented by Fe–N–C catalysts, have emerged and become a hot research topic in recent years. Although the initial activity of PGM-free catalysts has been significantly improved, it remains far behind that of state-of-the-art Pt catalysts [240]. Importantly, PGM-free catalysts degrade severely during PEM fuel cell operation, which presents the primary bottleneck for deploying PGM-free catalysts [60, 241].

For membranes and ionomers, PFSAs are the most popular polymer materials for PEM fuel cells. However, the PFSAs must be employed in a restricted operating condition, e.g., the temperature range, so that the performance can reach a high level. However, the optimal working conditions for membranes/ionomers are usually different from those for PEM fuel cells. This dilemma has triggered wide interest in exploring advanced membrane/ionomer working under broad working conditions. For example, novel hydrocarbon-based ionomers have been proposed, which are promising to not only overcome these limitations but also show considerable performance approaching PFSA-based materials. However, this type of ionomer is still not mature for scale-up applications.

Another key material discussed in this review article is the GDL, which primarily consists of carbon cloth, carbon paper, or carbon felt due to its high gas permeability, impressive strength and elasticity under compression, corrosion resistance in an acidic environment, and excellent electrical conductivity. Typically, the GDL thickness is between 200 and 400 μm. The GDL is essential for water management during fuel cell operation, while the MPL plays an important role in the transport of reactant gases and liquid water. However, the optimal porosity and pore size distribution, which limit the development of the GDL, have still not been widely agreed upon.

4.2 MEA Manufacturing Processing Constraints

In an MEA manufacturing line, the pivotal steps that significantly determine the quality of final products include ink dispersing and coating. For catalyst ink, agglomeration can lead to clogged nozzles. Conventional, the dispersion property has been an intensively focus for fresh catalyst ink. Otherwise, this "catalyst ink stability" concept has not been widely studied. We consider ink stability as a capability to resist aggregation, agglomeration, flocculation, coalescence, sedimentation, floatation, and/or creaming. The stability of the catalyst ink changes with time. When catalyst ink decays, an external shear force is needed to break up the aggregates and redisperse the particles, leading to a waste of time and labor. To date, there are two efficient approaches for controlling the dispersion state and stability. The composition of catalyst ink, such as the type of carbon support, the *I*/*C* ratio, and the type of solvent, remarkably affects ink properties and stability, as discussed in Sect. 3.1.1. Moreover, the ink preparation methods also strongly determine the ink properties and stability. Notably, a long dispersion time is usually required to obtain catalyst slurry with high stability, although a long dispersion time will increase the preparation cost and decrease the production efficiency. Recently, probe sonication was found to be highly efficient in preparing a highly stable colloidal ink [166]. One may suggest using high-viscosity catalyst ink to yield good stability. However, this would lead to difficulties during coating. At present, the ink preparation step presents its own challenges in high-efficiency dispersion and low processing cost. In addition,

an advanced technique is required to evaluate the stability of the catalyst ink. The rheological properties of catalyst ink play a critical role in catalyst layer formation, which can reflect the microstructure information, so rheology testing is needed to quantitatively probe the bulk microstructure and stability of inks [176]. For example, analytical centrifugation (AC) is a nondestructive technique to study particle migration behavior [166]; X-ray computed tomography (CT) is also useful in observing the interior changes of catalyst ink over time [190].

For large-scale catalyst coating, using continuous R2R technology is necessary. It should be noted that rolling can increase the contact area between the catalyst layer and PEM, thus reducing the contact resistance [242]. The primary challenges for R2R coating include: (1) precise transmission and continuous lamination of ultrathin flexible substrates; (2) synergy control and manipulation of picking-up, alignment, levelling, laminating, and die-cutting; (3) high precision half-die-cutting of flexible sealing film; (4) online image capturing and microcrack detection; (5) membrane cross section changing in MEA process; (6) microtension control of ultrathin film; (7) uniformity of hot-pressing and temperature controlling; and (8) clamping of coarse-fragile-porous media [231]. In particular, the swelling of the proton exchange membrane during the coating process must be considered for CCM production. During CCM, the catalyst ink is directly coated onto the membrane, whereby the solvent causes swelling and distortion. Swelling of the membrane is the primary cause of coating defects. To alleviate swelling issues, the compatibility between the catalyst ink (the solvent, to be specific) and membranes is important. If the catalyst ink contains too much solvent, it is more likely to swell the PEM. In this regard, the solvent content in catalyst ink should be optimized. On the other hand, the membrane must fit its backing film. Commercial PEMs are usually laminated to a backing film (PET and other materials). During coating, the adhesion between PEM and PET should be maintained at a certain strength to reduce the swelling of the membrane film. Meanwhile, the adhesion should not be too strong, as this would lead to difficulty in peeling off the membrane from the backing film [233]. In addition, for the popular slot-die coating technique, inhomogeneities can be observed [201]. Thus, more advanced coating strategies are required to control the quality of the catalyst layer, such as coating under stretched conditions [243].

5 Advanced Strategies to Integrate Key Materials into MEAs

Although a tremendous number of advanced materials, including catalysts, membranes, ionomers, GDLs, etc., have been developed for MEAs in PEM fuel cells, it remains a huge barrier to integrating these materials, especially newly developed ones, into practical MEAs. The MEA needs to be evaluated under different working conditions by using simplified testing protocols (e.g., a three-electrode system for catalyst testing) that are widely established in R&D settings. Therefore, the performance of key materials in laboratories cannot be completely reproduced in MEAs. However, the integration of materials into one MEA usually leads to performance loss. For example, the existence of ionomers in catalyst layers can cover the Pt sites and block reactions. This problem is not reflected by the conventionally used rotating disk electrode for ORR activity evaluation. In such circumstances, efficient strategies should be determined to integrate well-developed materials into MEAs. We believe that the following aspects are particularly important to future R&D.

5.1 Catalyst Ink Stability

Ink is usually overlooked when discussing about MEA integration. In fact, the properties of the catalyst ink greatly determine the catalyst layer quality. In the real-world large-scale MEA manufacturing process, catalyst inks need to be stocked to satisfy uninterrupted production requirements, and a certain storage time is needed. During storage, the catalyst ink should ideally be uniform, yet always suffers from agglomeration and even sedimentation because it is a heterogeneous material. Therefore, ink stability and the capability of particles to remain dispersed in the dispersion medium are vital for large-scale manufacturing. To improve the stability of catalyst ink, efforts can be made to (1) advance catalyst ink dispersion techniques, (2) optimize catalyst ink formula, (3) develop novel dispersants and additives, and (4) suitably define storage conditions of catalyst ink [189, 244, 245].

As discussed in Sect. 2.2, the SSC PFSA ionomer offers better performance than long-branched resins, i.e., LSC PFSA, especially under high-temperature and low-humidity working conditions [246]. However, it has been found that the catalyst ink prepared by using SSC ionomer shows lower stability. During storage, SSC ionomers tend to adhere to the catalyst surface so that the percentage of free ionomers decreases, thus destabilizing the catalyst ink [247]. In this regard, the LSC ionomer can benefit the stability of the catalyst ink. Even if the catalyst ink with the LSC ionomer degrades, its properties can be quickly recovered to initial states [247]. Therefore, efforts can be made to balance the ink properties and ink stability by using different ionomers.

5.2 Catalyst Layer Engineering

We highlight the current status that the excellent performance of key materials, particularly the catalyst, cannot be completely reproduced when they are integrated into

an MEA, especially when the Pt loading is low [248]. The greatest challenge is active site blocking by ionomers. Therefore, this issue is potentially addressed by not only preparing well-defined catalyst ink (discussed above) but also constructing well-defined three-phase boundaries (discussed below) to increase the catalyst utilization rate in the catalyst layer [249].

The conventional ink coating process leads to a random distribution of catalysts and ionomers. These ionomers may block active sites and pores in the catalyst layer, which thus presents insufficient channels for gas transport, electron conduction, and proton migration [250]. To address this issue, the concept of an ordered catalyst layer was proposed, which could provide independent channels [251].

Mathematical models have been established to simulate oxygen transport, proton conduction, and ordered catalytic layers. Du et al. reported a steady-state one-dimensional numerical model based on a cylindrical electrode structure to analyze the performance of the ordered cathode catalyst layer. The simulation results revealed that the ordered catalyst layers show better performance than conventional catalyst layers due to the improvements in mass transport and the uniformity of the electrochemical reaction rate across the whole width of the catalyst layer [252]. In 2006, they further proposed two steady-state one-dimensional models for the cathode catalyst layer, where the polarization curves were simulated, predicting a superior performance compared to the conventional catalyst layer model, even using lower Pt loadings. The detailed analysis indicated that the improved performance of the ordered catalyst layer can be primarily attributed to the uniform distributions of oxygen concentration and overpotential [253]. In addition, a 3D mathematical model of an ordered nanostructured cathode catalyst layer was studied. In the absence of liquid water, oxygen diffusion in the pore phase was not the limiting factor, due to its parallel gas pores [254]. In practice, the ordered catalyst layer has proven helpful in improving fuel cell performance. For the first time, in 2002, an order-structured catalyst layer with perpendicular channels was proposed for electron, proton, gas, and water transportation [255]. By applying ordered Pt nanotube arrays in a nanostructured ultrathin catalyst layer, the MEA exhibited remarkable improvements in terms of specific activity and mass transportation compared with the state-of-the-art randomly distributed Pt/C catalyst layer [256].

To date, the ordered catalyst layer has attracted tremendous attention. The ordered catalyst layer can be achieved through two designs: the aligned electrolyte framework and the aligned catalyst framework (Fig. 24).

A successful example of the aligned electrolyte framework concept is the pillar-structured membrane. For example, ordered micropillar arrays are patterned on a membrane surface by imprint/micromould lithography; therefore, reactant transport losses are reduced and performance is

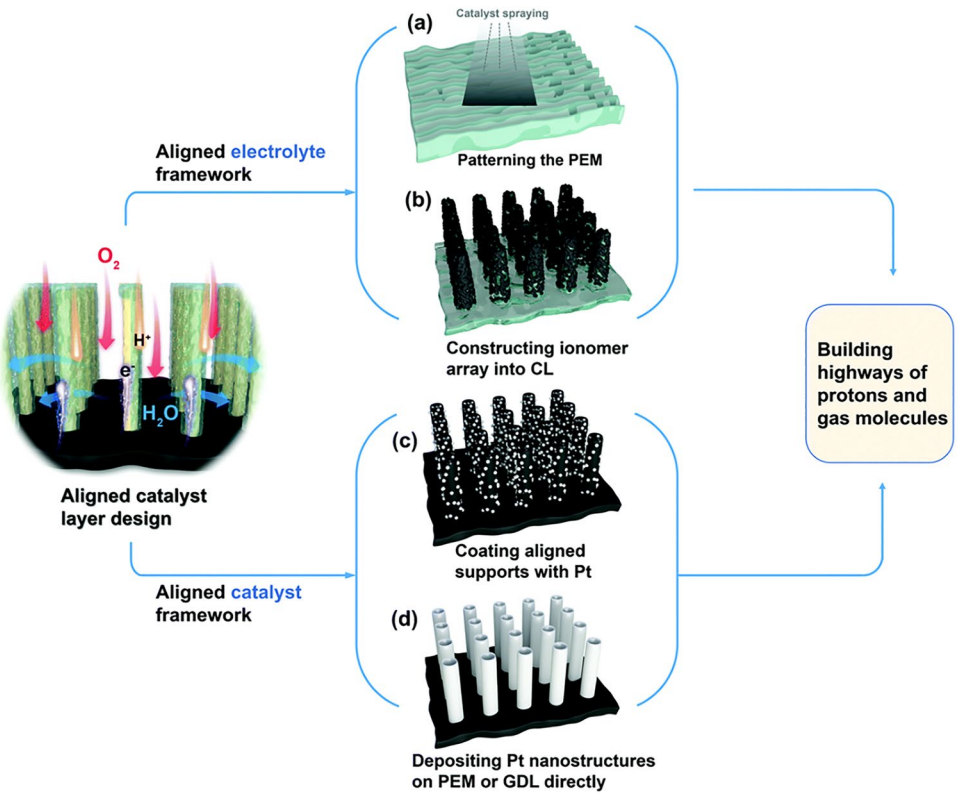

Fig. 24 Schematic diagrams of the aligned CLs with (**a** and **b**) electrolyte and (**c** and **d**) catalysts as frameworks. Reprinted with permission from Ref. [102]. Copyright © 2022, The Royal Society of Chemistry

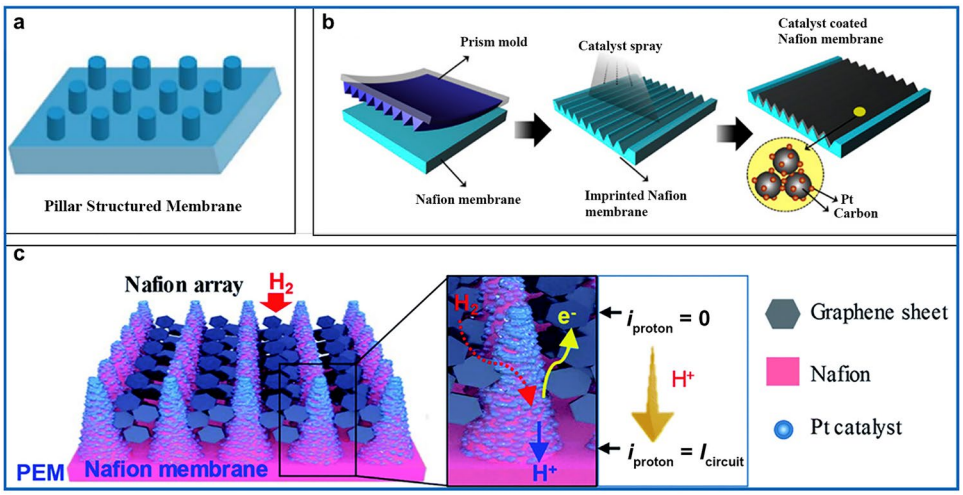

Fig. 25 Illustrative structure for an aligned electrolyte framework, **a** pillar-structured membrane. Reprinted with permission from Ref. [257]. Copyright © 2010, The Electrochemical Society. **b** Prism-patterned array Nafion membrane. Reprinted with permission from Ref. [258]. Copyright © 2016, Elsevier B.V. **c** Well-ordered and cone-shaped Nafion array membrane. Reprinted with permission from Ref. [259]. Copyright © 2020, The Royal Society of Chemistry

enhanced [257] (Fig. 25a). Moreover, the ordered catalyst layer benefits water management, including fast removal of generated water and avoidance of flooding. For example, imprinting prism-patterned arrays onto the Nafion membrane was reported (Fig. 25b). Compared to the pillar structure, this vertically asymmetric geometry of the prism structure remarkably enhanced water transportation [258]. Very recently, a well-ordered and cone-shaped Nafion array membrane was proposed and prepared using an anodic aluminum oxide (AAO) template (Fig. 25c). The Pt nanocatalyst was directly deposited on the Nafion array, which effectively solved the problem of filling the catalyst into the dense array [259].

The aligned catalyst framework concept has been intensively studied [260]. Usually, aligned carbon nanotubes or nanofibers, conducting metal dioxides (e.g., TiO_2 and SnO_2), and conductive polymers can be used as supports for Pt nanoparticles and are employed as ordered catalyst supports for PEMFCs to yield ordered catalytic layer structures [261–263] such as the nanostructured thin film (NSTF) electrode developed by 3M Company. The NSTF electrode is an ultrathin electrode covered with a continuous thin Pt or Pt alloy catalyst [264], where the support is a crystalline organic pigment material (namely, nanowhiskers) [265]. In addition, the electronic conductive polymer polypyrrole (PPy) nanowire can also be employed as the ordered catalyst support [266]. The fabricated single cell with an ordered catalyst layer that uses less ionomer typically presents much better mass transport in the high current density range, which is even superior to the commercial Pt/C-based electrode under certain operating conditions.

Notably, the ordered catalyst layer may be difficult to scale up. Beyond the ordered catalyst layer, which can build independent transfer channels for electrons, protons, oxygen, and water, the multilayer catalyst layer structure (including the gradient catalyst layer) is another choice. This material should be easier to fabricate by using current MEA manufacturing lines.

The catalyst layer (CL) contacts the PEM on one side and the GDL on the other side, forming a PEM/CL/GDL structure (Fig. 1b, c). This configuration demands different features for different parts of the catalyst layer. At the PEM/CL interface where mass current is generated, sufficient ionic conductivity is needed, whereas abundant porosity is needed at the CL/GDL interface to allow for fast gas transport. A changing composition perpendicular to the CL interfaces cannot be achieved in the conventional catalyst layers consisting of homogeneously distributed catalyst and ionomer. For example, the Nafion content in the PEM/CL interface is optimal for proton transportation yet is too high in the CL/GDL interface and leads to flooding and increased gas diffusion resistance [220]. Additionally, the multilayer catalyst layer can provide more three-phase boundaries. For example, the design of the Pt layer/Nafion–carbon (without Pt) layer was alternatively suggested to attain a more continuous three-dimensional reaction zone [267]. In practice, applying a multilayer design in the catalyst layer can also precisely control the internal architecture in the catalyst layer in three dimensions [268].

To build a multilayer/gradient catalyst layer, changing the ionomer content [269], Pt loading [249], and both [270] has been investigated. In addition, changing the catalyst support was also reported. As shown in Fig. 26a–c, different catalyst supports, including a high microporosity carbon (Ketjen Black EC-300J) and a low porosity carbon (XC-72 Vulcan carbon), were applied to build a dual-layer catalyst layer. The dual-layer design remarkably improved the fuel cell performance compared to the one using mixed catalysts. Surprisingly, the position of Pt/VC or Pt/KB had no major impact on cell performance [220].

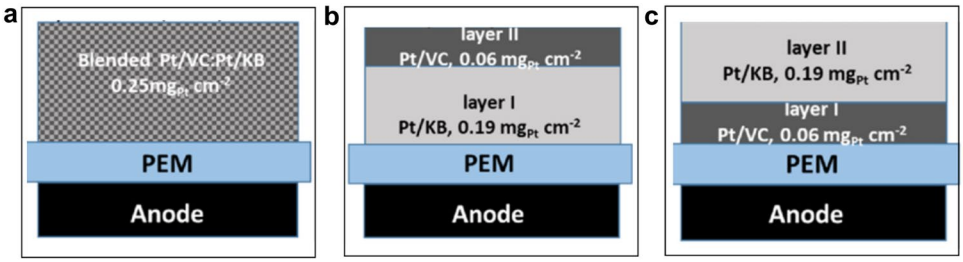

Fig. 26 Illustrations of the three different cathode catalyst layers used. Reprinted with permission from Ref. [220]. Copyright © 2021, Elsevier B.V.

6 Summary and Outlook

This review presents advances in key materials (Sect. 2), including catalysts, membranes, ionomers, and GDLs and state-of-the-art MEA manufacturing processing (Sect. 3). Overall, the development from materials to MEA is inspiring and has efficiently advanced the R&D of PEM fuel cells. However, limitations in materials and MEA manufacturing still exist (Sect. 4) and deserve more effort to resolve. Despite these material constraints, we focus on the gaps precluding materials from integration into MEAs. Therefore, we provide a discussion on strategies to enable emerging material integration (Sect. 5).

In addition to the above discussion, the following aspects may be instructive for future PEM fuel cell R&D.

Development of new materials. In this review paper, we primarily focus on "mature materials" that have been used in industrial production. It is noteworthy that the development of fuel cell techniques historically relied on the development of new materials. Therefore, intelligent design and synthesis of new materials, including catalysts, membranes, ionomers, GDLs, etc., should be a focus of future PEM fuel cell studies. We emphasize that newly developed materials with good performance in replicating practical conditions (e.g., the catalyst research using RDE equipment) are not always suitable for use in MEA. The evaluation of new materials must also be performed in real-world MEA.

Deep understanding of key materials. PEM fuel cells incorporate many key materials. In particular, catalysts, membranes/ionomers, and GDLs with better performance, higher stability, and lower cost are highly desired. For the development of these materials, fundamental understanding, in terms of the characteristic–performance relationship, characteristics changing over time, and performance under different operating conditions, is needed. However, deep understanding in these fields is still to be developed. In particular, efficient research methods/tools are still lacking for working MEAs. This highly requires in situ/operando characterization tools, especially those that can be used for testing MEAs under real-world operating conditions. Accordingly, theoretical calculation approaches would be helpful supplementary to assist fundamental research.

Materials integration into the MEAs. Integrating key materials into an MEA is important in the PEM fuel cell field. Toward this goal, a significant problem is that good performance of materials by replication testing of real-world MEAs cannot easily be achieved. Building a well-defined, highly ordered catalyst layer thus attracts great interest. In general, first-generation MEA fabrication is based on CCS, while second-generation MEA fabrication (the state-of-the-art method) is based on CCM. Given the latest advances in building highly ordered catalyst layers, we believe that next-generation MEA production lines could be based on oriented catalyst layer engineering. In this regard, R&D of the corresponding prototype processes might be needed.

Automatic manufacturing. The development of PEM fuel cells is based on the underlying materials. Automatic manufacturing processes will become extremely important when PEM fuel cells are widely deployed. Current production lines for materials and MEAs are not fully automatic. To save labor and improve production efficiency and product yield, automatic manufacturing is essential.

Scale-up application of PEM fuel cells. At present, many PEM fuel cell applications are operating globally. However, the volume remains tiny compared to combustion engine and battery manufacturing. This reality limits the diversity of ancillary facilities and discourages enthusiasm to apply fuel cell devices. Government-leading large-scale PEM fuel cell efforts are necessary. Scaling up the application of PEM fuel cells can build a new industrial chain around "hydrogen energy". Furthermore, the resulting mass of data describing operating cells can be collected and fed back to the manufacturing channels, which will help in developing better cells. For such R&D efforts, analyzing big data by using artificial intelligence is a future direction.

Acknowledgements This work was supported by the National Key Research and Development Program of China (No. 2020YFB1505800), the National Natural Science Foundation of China (No. 22250710133 and 51803042), Outstanding Youth Project of Natural Science Foundation of Guangdong Province (No. 2022B1515020020), Funding by Science and Technology Projects in Guangzhou (No. 202206050003 and 202201010603) and Guangdong Engineering Technology Research Center for Hydrogen Energy and Fuel Cells.

Ethics statement The authors declare that they have no conflict of interests. Siyu Ye is an editorial board member for *Electrochemical Energy Reviews* and was not involved in the editorial review or the decision to publish this article.

References

1. Cano, Z.P., Banham, D., Ye, S.Y., et al.: Batteries and fuel cells for emerging electric vehicle markets. Nat. Energy **3**, 279–289 (2018). https://doi.org/10.1038/s41560-018-0108-1
2. Wang, Y., Ruiz Diaz, D.F., Chen, K.S., et al.: Materials, technological status, and fundamentals of PEM fuel cells: a review. Mater. Today **32**, 178–203 (2020). https://doi.org/10.1016/j.mattod.2019.06.005
3. Zhang, J., Hu, Y.: Sealing performance and mechanical behavior of PEMFCs sealing system based on thermodynamic coupling. Int. J. Hydrog. Energy **45**, 23480–23489 (2020). https://doi.org/10.1016/j.ijhydene.2020.06.167
4. Chen, Y.X., Singh, Y., Ramani, D., et al.: 4D imaging of chemo-mechanical membrane degradation in polymer electrolyte fuel cells. Part 1: understanding and evading edge failures. J. Power Sources **520**, 230674 (2022). https://doi.org/10.1016/j.jpowsour.2021.230674
5. Schulze, M., Knöri, T., Schneider, A., et al.: Degradation of sealings for PEFC test cells during fuel cell operation. J. Power Sources **127**, 222–229 (2004). https://doi.org/10.1016/j.jpowsour.2003.09.017
6. Yue, W., Qiu, D.K., Yi, P.Y., et al.: Study on the degradation mechanism of the frame for membrane electrode assembly in proton exchange membrane fuel cell. Int. J. Hydrog. Energy **46**, 36954–36968 (2021). https://doi.org/10.1016/j.ijhydene.2021.08.204
7. Ye, D.H., Zhan, Z.G., Lee, Y.J., et al.: Effects of frame materials and structures on stress concentration of membrane electrode assembly of PEMFCs. Fuel Cells **13**, 1205–1212 (2013). https://doi.org/10.1002/fuce.201300073
8. Ye, D.H., Zhan, Z.G.: A review on the sealing structures of membrane electrode assembly of proton exchange membrane fuel cells. J. Power Sources **231**, 285–292 (2013). https://doi.org/10.1016/j.jpowsour.2013.01.009
9. Liang, P., Qiu, D.K., Peng, L.F., et al.: Structure failure of the sealing in the assembly process for proton exchange membrane fuel cells. Int. J. Hydrog. Energy **42**, 10217–10227 (2017). https://doi.org/10.1016/j.ijhydene.2017.01.026
10. Qiu, D.K., Peng, L.F., Lai, X.M., et al.: Mechanical failure and mitigation strategies for the membrane in a proton exchange membrane fuel cell. Renew. Sustain. Energy Rev. **113**, 109289 (2019). https://doi.org/10.1016/j.rser.2019.109289
11. Tzelepis, S., Kavadias, K.A., Marnellos, G.E., et al.: A review study on proton exchange membrane fuel cell electrochemical performance focusing on anode and cathode catalyst layer modelling at macroscopic level. Renew. Sustain. Energy Rev. **151**, 111543 (2021). https://doi.org/10.1016/j.rser.2021.111543
12. Du, L., Du, C.Y., Chen, G.Y., et al.: Metal-organic coordination networks: Prussian blue and its synergy with Pt nanoparticles to enhance oxygen reduction kinetics. ACS Appl. Mater. Interfaces **8**, 15250–15257 (2016). https://doi.org/10.1021/acsami.6b02630
13. Du, L., Kong, F.P., Chen, G.Y., et al.: A review of applications of poly(diallyldimethyl ammonium chloride) in polymer membrane fuel cells: from nanoparticles to support materials. Chin. J. Catal. **37**, 1025–1036 (2016). https://doi.org/10.1016/S1872-2067(16)62480-4
14. Sun, S.H., Zhang, G.X., Gauquelin, N., et al.: Single-atom catalysis using Pt/graphene achieved through atomic layer deposition. Sci. Rep. **3**, 1–9 (2013). https://doi.org/10.1038/srep01775
15. Yu, X.W., Ye, S.Y.: Recent advances in activity and durability enhancement of Pt/C catalytic cathode in PEMFC. J. Power Sources **172**, 133–144 (2007). https://doi.org/10.1016/j.jpowsour.2007.07.049
16. Song, Z.X., Norouzi Banis, M., Liu, H.S., et al.: Ultralow loading and high-performing Pt catalyst for a polymer electrolyte membrane fuel cell anode achieved by atomic layer deposition. ACS Catal. **9**, 5365–5374 (2019). https://doi.org/10.1021/acscatal.8b04504
17. Du, L., Zhang, S., Chen, G.Y., et al.: Polyelectrolyte assisted synthesis and enhanced oxygen reduction activity of Pt nanocrystals with controllable shape and size. ACS Appl. Mater. Interfaces **6**, 14043–14049 (2014). https://doi.org/10.1021/am503372f
18. Yu, X.W., Ye, S.Y.: Recent advances in activity and durability enhancement of Pt/C catalytic cathode in PEMFC. J. Power Sources **172**, 145–154 (2007). https://doi.org/10.1016/j.jpowsour.2007.07.048
19. Cullen, D.A., Neyerlin, K.C., Ahluwalia, R.K., et al.: New roads and challenges for fuel cells in heavy-duty transportation. Nat. Energy **6**, 462–474 (2021). https://doi.org/10.1038/s41560-021-00775-z
20. Zhao, Z.P., Liu, Z.Y., Zhang, A., et al.: Graphene-nanopocket-encaged PtCo nanocatalysts for highly durable fuel cell operation under demanding ultralow-Pt-loading conditions. Nat. Nanotechnol. **17**, 968–975 (2022). https://doi.org/10.1038/s41565-022-01170-9
21. Du, L., Shao, Y.Y., Sun, J.M., et al.: Advanced catalyst supports for PEM fuel cell cathodes. Nano Energy **29**, 314–322 (2016). https://doi.org/10.1016/j.nanoen.2016.03.016
22. Ren, P., Pei, P.C., Li, Y.H., et al.: Degradation mechanisms of proton exchange membrane fuel cell under typical automotive operating conditions. Prog. Energy Combust. Sci. **80**, 100859 (2020). https://doi.org/10.1016/j.pecs.2020.100859
23. Kong, F.P., Ren, Z.H., Norouzi Banis, M., et al.: Active and stable Pt–Ni alloy octahedra catalyst for oxygen reduction via near-surface atomical engineering. ACS Catal. **10**, 4205–4214 (2020). https://doi.org/10.1021/acscatal.9b05133
24. Tian, X.L., Zhao, X., Su, Y.Q., et al.: Engineering bunched Pt–Ni alloy nanocages for efficient oxygen reduction in practical fuel cells. Science **366**, 850–856 (2019). https://doi.org/10.1126/science.aaw7493
25. Zheng, Z.F., Luo, L.X., Zhu, F.J., et al.: Degradation of core–shell Pt_3Co catalysts in proton exchange membrane fuel cells (PEMFCs) studied by mathematical modeling. Electrochim. Acta **323**, 134751 (2019). https://doi.org/10.1016/j.electacta.2019.134751
26. Lyu, X., Jia, Y., Mao, X., et al.: Gradient-concentration design of stable core–shell nanostructure for acidic oxygen reduction electrocatalysis. Adv. Mater. **32**, e2003493 (2020). https://doi.org/10.1002/adma.202003493

27. Huang, J., Peng, B.S., Stracensky, T., et al.: 1D PtCo nanowires as catalysts for PEMFCs with low Pt loading. Sci. China Mater. **65**, 704–711 (2022). https://doi.org/10.1007/s40843-021-1777-x
28. Jiang, K.Z., Zhao, D.D., Guo, S.J., et al.: Efficient oxygen reduction catalysis by subnanometer Pt alloy nanowires. Sci. Adv. **3**, e1601705 (2017). https://doi.org/10.1126/sciadv.1601705
29. Hoque, M.A., Hassan, F.M., Jauhar, A.M., et al.: Web-like 3D architecture of Pt nanowires and sulfur-doped carbon nanotube with superior electrocatalytic performance. ACS Sustain. Chem. Eng. **6**, 93–98 (2018). https://doi.org/10.1021/acssuschemeng.7b03580
30. Bu, L.Z., Zhang, N., Guo, S.J., et al.: Biaxially strained PtPb/Pt core/shell nanoplate boosts oxygen reduction catalysis. Science **354**, 1410–1414 (2016). https://doi.org/10.1126/science.aah6133
31. Yang, J., Hübner, R., Zhang, J.W., et al.: A robust PtNi nanoframe/N-doped graphene aerogel electrocatalyst with both high activity and stability. Angew. Chem. Int. Ed. **60**, 9590–9597 (2021). https://doi.org/10.1002/anie.202015679
32. Luo, S.P., Tang, M., Shen, P.K., et al.: Atomic-scale preparation of octopod nanoframes with high-index facets as highly active and stable catalysts. Adv. Mater. **29**, 1601687 (2017). https://doi.org/10.1002/adma.201601687
33. Li, M.F., Zhao, Z.P., Cheng, T., et al.: Ultrafine jagged platinum nanowires enable ultrahigh mass activity for the oxygen reduction reaction. Science **354**, 1414–1419 (2016). https://doi.org/10.1126/science.aaf9050
34. Zhang, L., Liu, H.S., Liu, S.H., et al.: Pt/Pd single-atom alloys as highly active electrochemical catalysts and the origin of enhanced activity. ACS Catal. **9**, 9350–9358 (2019). https://doi.org/10.1021/acscatal.9b01677
35. Hammer, B., Norskov, J.K.: Why gold is the noblest of all the metals. Nature **376**, 238–240 (1995). https://doi.org/10.1038/376238a0
36. Medford, A.J., Vojvodic, A., Hummelshøj, J.S., et al.: From the Sabatier principle to a predictive theory of transition-metal heterogeneous catalysis. J. Catal. **328**, 36–42 (2015). https://doi.org/10.1016/j.jcat.2014.12.033
37. Stamenkovic, V., Mun, B.S., Mayrhofer, K.J.J., et al.: Changing the activity of electrocatalysts for oxygen reduction by tuning the surface electronic structure. Angew. Chem. Int. Ed. **45**, 2897–2901 (2006). https://doi.org/10.1002/anie.200504386
38. Greeley, J., Jaramillo, T.F., Bonde, J., et al.: Computational high-throughput screening of electrocatalytic materials for hydrogen evolution. Nat. Mater. **5**, 909–913 (2006). https://doi.org/10.1038/nmat1752
39. Chong, L.N., Wen, J.G., Kubal, J., et al.: Ultralow-loading platinum–cobalt fuel cell catalysts derived from imidazolate frameworks. Science **362**, 1276–1281 (2018). https://doi.org/10.1126/science.aau0630
40. Antolini, E.: Alloy vs. intermetallic compounds: effect of the ordering on the electrocatalytic activity for oxygen reduction and the stability of low temperature fuel cell catalysts. Appl. Catal. B Environ. **217**, 201–213 (2017). https://doi.org/10.1016/j.apcatb.2017.05.081
41. Li, J.R., Sharma, S., Liu, X.M., et al.: Hard-magnet $L1_0$-CoPt nanoparticles advance fuel cell catalysis. Joule **3**, 124–135 (2019). https://doi.org/10.1016/j.joule.2018.09.016
42. Yang, C.L., Wang, L.N., Yin, P., et al.: Sulfur-anchoring synthesis of platinum intermetallic nanoparticle catalysts for fuel cells. Science **374**, 459–464 (2021). https://doi.org/10.1126/science.abj9980
43. Sievers, G.W., Jensen, A.W., Quinson, J., et al.: Self-supported Pt–CoO networks combining high specific activity with high surface area for oxygen reduction. Nat. Mater. **20**, 208–213 (2021). https://doi.org/10.1038/s41563-020-0775-8
44. Du, L., Zhang, G.X., Sun, S.H.: Proton exchange membrane (PEM) fuel cells with platinum group metal (PGM)-free cathode. Automot. Innov. **4**, 131–143 (2021). https://doi.org/10.1007/s42154-021-00146-0
45. Du, L., Xing, L.X., Zhang, G.X., et al.: Strategies for engineering high-performance PGM-free catalysts toward oxygen reduction and evolution reactions. Small Methods **4**, 2000016 (2020). https://doi.org/10.1002/smtd.202000016
46. Qiao, B.T., Wang, A.Q., Yang, X.F., et al.: Single-atom catalysis of CO oxidation using Pt_1/FeO_x. Nat. Chem. **3**, 634–641 (2011). https://doi.org/10.1038/nchem.1095
47. Du, L., Zhang, G.X., Liu, X.H., et al.: Biomass-derived nonprecious metal catalysts for oxygen reduction reaction: the demand-oriented engineering of active sites and structures. Carbon Energy **2**, 561–581 (2020). https://doi.org/10.1002/cey2.73
48. Shao, Y.Y., Dodelet, J.P., Wu, G., et al.: PGM-free cathode catalysts for PEM fuel cells: a mini-review on stability challenges. Adv. Mater. **31**, 1807615 (2019). https://doi.org/10.1002/adma.201807615
49. Holby, E.F., Wang, G.F., Zelenay, P.: Acid stability and demetalation of PGM-free ORR electrocatalyst structures from density functional theory: a model for "single-atom catalyst" dissolution. ACS Catal. **10**, 14527–14539 (2020). https://doi.org/10.1021/acscatal.0c02856
50. Zhang, H.G., Osgood, H., Xie, X.H., et al.: Engineering nanostructures of PGM-free oxygen-reduction catalysts using metal–organic frameworks. Nano Energy **31**, 331–350 (2017). https://doi.org/10.1016/j.nanoen.2016.11.033
51. Wang, X.X., Swihart, M.T., Wu, G.: Achievements, challenges and perspectives on cathode catalysts in proton exchange membrane fuel cells for transportation. Nat. Catal. **2**, 578–589 (2019). https://doi.org/10.1038/s41929-019-0304-9
52. Zhang, H.G., Chung, H.T., Cullen, D.A., et al.: High-performance fuel cell cathodes exclusively containing atomically dispersed iron active sites. Energy Environ. Sci. **12**, 2548–2558 (2019). https://doi.org/10.1039/C9EE00877B
53. Gollasch, M., Müller-Hülstede, J., Schmies, H., et al.: Elucidating synergistic effects of different metal ratios in bimetallic Fe/Co–N–C catalysts for oxygen reduction reaction. Catalysts **11**, 841 (2021). https://doi.org/10.3390/catal11070841
54. Han, Y., Yin, S.H., Chen, Y.H., et al.: Experimental and DFT studies of oxygen reduction reaction promoted by binary site Fe/Co–N–C catalyst in acid. J. Electroanal. Chem. **914**, 116322 (2022). https://doi.org/10.1016/j.jelechem.2022.116322
55. Wang, N., Tang, C.M., Du, L., et al.: Advanced cathode materials for protonic ceramic fuel cells: recent progress and future perspectives. Adv. Energy Mater. **12**, 2201882 (2022). https://doi.org/10.1002/aenm.202201882
56. Wang, N., Yuan, B.Y., Tang, C.M., et al.: Machine-learning-accelerated development of efficient mixed protonic-electronic conducting oxides as the air electrodes for protonic ceramic cells. Adv. Mater. **34**, e2203446 (2022). https://doi.org/10.1002/adma.202203446
57. Ding, R., Wang, R., Ding, Y.Q., et al.: Designing AI-aided analysis and prediction models for nonprecious metal electrocatalyst-based proton-exchange membrane fuel cells. Angew. Chem. Int. Ed. **59**, 19175–19183 (2020). https://doi.org/10.1002/anie.202006928
58. Zhao, S.N., Li, J.K., Wang, R., et al.: Electronically and geometrically modified single-atom Fe sites by adjacent Fe nanoparticles for enhanced oxygen reduction. Adv. Mater. **34**, 2107291 (2022). https://doi.org/10.1002/adma.202107291
59. Liu, S.W., Li, C.Z., Zachman, M.J., et al.: Atomically dispersed iron sites with a nitrogen–carbon coating as highly active and durable oxygen reduction catalysts for fuel cells. Nat. Energy **7**, 652–663 (2022). https://doi.org/10.1038/s41560-022-01062-1

60. Du, L., Prabhakaran, V., Xie, X.H., et al.: Low-PGM and PGM-free catalysts for proton exchange membrane fuel cells: stability challenges and material solutions. Adv. Mater. **33**, e1908232 (2021). https://doi.org/10.1002/adma.201908232
61. Sun, W., Du, L., Tan, Q., et al.: Engineering of nitrogen coordinated single cobalt atom moieties for oxygen electroreduction. ACS Appl. Mater. Interfaces **11**, 41258–41266 (2019). https://doi.org/10.1021/acsami.9b11830
62. Xing, Z.H., Xiao, M.L., Guo, Z.L., et al.: Colloidal silica assisted fabrication of N, O, S-tridoped porous carbon nanosheets with excellent oxygen reduction performance. Chem. Commun. (Camb) **54**, 4017–4020 (2018). https://doi.org/10.1039/c8cc00846a
63. Xing, Z.H., Jin, R., Chen, X.Y., et al.: Self-templating construction of N, P-co-doped carbon nanosheets for efficient eletreocatalytic oxygen reduction reaction. Chem. Eng. J. **410**, 128015 (2021). https://doi.org/10.1016/j.cej.2020.128015
64. An, F., Bao, X.Q., Deng, X.Y., et al.: Carbon-based metal-free oxygen reduction reaction electrocatalysts: past, present and future. New Carbon Mater. **37**, 338–354 (2022). https://doi.org/10.1016/S1872-5805(22)60590-0
65. Kongkanand, A., Mathias, M.F.: The priority and challenge of high-power performance of low-platinum proton-exchange membrane fuel cells. J. Phys. Chem. Lett. **7**, 1127–1137 (2016). https://doi.org/10.1021/acs.jpclett.6b00216
66. Fan, J.T., Chen, M., Zhao, Z.L., et al.: Bridging the gap between highly active oxygen reduction reaction catalysts and effective catalyst layers for proton exchange membrane fuel cells. Nat. Energy **6**, 475–486 (2021). https://doi.org/10.1038/s41560-021-00824-7
67. Parnian, M.J., Rowshanzamir, S., Prasad, A.K., et al.: High durability sulfonated poly (ether etherketone)-ceria nanocomposite membranes for proton exchange membrane fuel cell applications. J. Membr. Sci. **556**, 12–22 (2018). https://doi.org/10.1016/j.memsci.2018.03.083
68. Nguyen, H., Klose, C., Metzler, L., et al.: Fully hydrocarbon membrane electrode assemblies for proton exchange membrane fuel cells and electrolyzers: an engineering perspective. Adv. Energy Mater. **12**, 2103559 (2022). https://doi.org/10.1002/aenm.202103559
69. Pan, M.Z., Pan, C.J., Li, C., et al.: A review of membranes in proton exchange membrane fuel cells: transport phenomena, performance and durability. Renew. Sustain. Energy Rev. **141**, 110771 (2021). https://doi.org/10.1016/j.rser.2021.110771
70. Ahluwalia, R., James, B., Houchins C., et al.: DOE hydrogen and fuel cells program record. https://www.hydrogen.energy.gov/pdfs/17007_fuel_cell_system_cost_2017.pdf (2017)
71. Ayers, K.: The potential of proton exchange membrane-based electrolysis technology. Curr. Opin. Electrochem. **18**, 9–15 (2019). https://doi.org/10.1016/j.coelec.2019.08.008
72. Ferrara, A., Polverino, P., Pianese, C.: Analytical calculation of electrolyte water content of a proton exchange membrane fuel cell for on-board modelling applications. J. Power Sources **390**, 197–207 (2018). https://doi.org/10.1016/j.jpowsour.2018.04.005
73. Alawajji, R.A., Kannarpady, G.K., Biris, A.S.: Fabrication of transparent superhydrophobic polytetrafluoroethylene coating. Appl. Surf. Sci. **444**, 208–215 (2018). https://doi.org/10.1016/j.apsusc.2018.02.206
74. Talukdar, K., Gazdzicki, P., Friedrich, K.A.: Comparative investigation into the performance and durability of long and short side chain ionomers in polymer electrolyte membrane fuel cells. J. Power Sources **439**, 227078 (2019). https://doi.org/10.1016/j.jpowsour.2019.227078
75. Giancola, S., Zatoń, M., Reyes-Carmona, Á., et al.: Composite short side chain PFSA membranes for PEM water electrolysis. J. Membr. Sci. **570**(571), 69–76 (2019). https://doi.org/10.1016/j.memsci.2018.09.063
76. Luo, X.Y., Holdcroft, S., Mani, A.N., et al.: Water, proton, and oxygen transport in high IEC, short side chain PFSA ionomer membranes: consequences of a frustrated network. Phys. Chem. Chem. Phys. **13**, 18055–18062 (2011). https://doi.org/10.1039/c1cp22559f
77. Beauger, C., Lainé, G., Burr, A., et al.: Improvement of Nafion®-sepiolite composite membranes for PEMFC with sulfo-fluorinated sepiolite. J. Membr. Sci. **495**, 392–403 (2015). https://doi.org/10.1016/j.memsci.2015.08.014
78. Li, T., Shen, J.B., Chen, G.Y., et al.: Performance comparison of proton exchange membrane fuel cells with Nafion and aquivion perfluorosulfonic acids with different equivalent weights as the electrode binders. ACS Omega **5**, 17628–17636 (2020). https://doi.org/10.1021/acsomega.0c02110
79. Tang, H.Y., Geng, K., Wu, L., et al.: Fuel cells with an operational range of − 20 ℃ to 200 ℃ enabled by phosphoric acid-doped intrinsically ultramicroporous membranes. Nat. Energy **7**, 153–162 (2022). https://doi.org/10.1038/s41560-021-00956-w
80. Liu, Y.X., Ye, J., Kong, F.P., et al.: Pt/C–TiO_2 as oxygen reduction electrocatalysts against sulfur poisoning. Catalysts **12**, 571 (2022). https://doi.org/10.3390/catal12050571
81. Liu, Y.X., Zhang, W.Y., Han, G.K., et al.: Deactivation and regeneration of a benchmark Pt/C catalyst toward oxygen reduction reaction in the presence of poisonous SO_2 and NO. Catal. Sci. Technol. **12**, 2929–2934 (2022). https://doi.org/10.1039/d2cy00141a
82. Liu, Y.X., Zhang, W.Y., Han, G.K., et al.: Deactivated Pt electrocatalysts for the oxygen reduction reaction: the regeneration mechanism and a regenerative protocol. ACS Catal. **11**, 9293–9299 (2021). https://doi.org/10.1021/acscatal.1c01680
83. Liu, Y.X., Du, L., Kong, F.P., et al.: Sulfur dioxide-tolerant bimetallic PtRu catalyst toward oxygen electroreduction. ACS Sustain. Chem. Eng. **8**, 1295–1301 (2020). https://doi.org/10.1021/acssuschemeng.9b06785
84. Alink, R., Gerteisen, D., Oszcipok, M.: Degradation effects in polymer electrolyte membrane fuel cell stacks by sub-zero operation: an in situ and ex situ analysis. J. Power Sources **182**, 175–187 (2008). https://doi.org/10.1016/j.jpowsour.2008.03.074
85. Yan, Q.G., Toghiani, H., Lee, Y.W., et al.: Effect of sub-freezing temperatures on a PEM fuel cell performance, startup and fuel cell components. J. Power Sources **160**, 1242–1250 (2006). https://doi.org/10.1016/j.jpowsour.2006.02.075
86. Bose, S., Kuila, T., Nguyen, T.X.H., et al.: Polymer membranes for high temperature proton exchange membrane fuel cell: recent advances and challenges. Prog. Polym. Sci. **36**, 813–843 (2011). https://doi.org/10.1016/j.progpolymsci.2011.01.003
87. Zhang, H.W., Shen, P.K.: Advances in the high performance polymer electrolyte membranes for fuel cells. Chem. Soc. Rev. **41**, 2382–2394 (2012). https://doi.org/10.1039/c2cs15269j
88. Shin, D.W., Guiver, M.D., Lee, Y.M.: Hydrocarbon-based polymer electrolyte membranes: importance of morphology on ion transport and membrane stability. Chem. Rev. **117**, 4759–4805 (2017). https://doi.org/10.1021/acs.chemrev.6b00586
89. Wong, C.Y., Wong, W.Y., Ramya, K., et al.: Additives in proton exchange membranes for low- and high-temperature fuel cell applications: a review. Int. J. Hydrog. Energy **44**, 6116–6135 (2019). https://doi.org/10.1016/j.ijhydene.2019.01.084
90. Qu, E.L., Hao, X.F., Xiao, M., et al.: Proton exchange membranes for high temperature proton exchange membrane fuel cells: challenges and perspectives. J. Power Sources **533**, 231386 (2022). https://doi.org/10.1016/j.jpowsour.2022.231386
91. Lim, K.H., Lee, A.S., Atanasov, V., et al.: Protonated phosphonic acid electrodes for high power heavy-duty vehicle fuel

cells. Nat. Energy **7**, 248–259 (2022). https://doi.org/10.1038/s41560-021-00971-x
92. Placca, L., Kouta, R.: Fault tree analysis for PEM fuel cell degradation process modelling. Int. J. Hydrog. Energy **36**, 12393–12405 (2011). https://doi.org/10.1016/j.ijhydene.2011.06.093
93. Curtin, D.E., Lousenberg, R.D., Henry, T.J., et al.: Advanced materials for improved PEMFC performance and life. J. Power Sources **131**, 41–48 (2004). https://doi.org/10.1016/j.jpowsour.2004.01.023
94. Wang, J., Dai, Y., Wan, R.Y., et al.: Grafting free radical scavengers onto polyarylethersulfone backbones for superior chemical stability of high temperature polymer membrane electrolytes. Chem. Eng. J. **413**, 127541 (2021). https://doi.org/10.1016/j.cej.2020.127541
95. Banham, D., Ye, S.Y., Cheng, T., et al.: Impact of CeO_x additives on cathode catalyst layer poisoning. ECS Trans. **58**, 369–380 (2013). https://doi.org/10.1149/05801.0369ecst
96. MacAuley, N., Lauritzen, M., Knights, S., et al.: Predicting membrane lifetime with cerium oxide in heavy duty fuel cell systems. J. Electrochem. Soc. **165**, F780–F785 (2018). https://doi.org/10.1149/2.0271810jes
97. Kumar, A., Hong, J., Yun, Y.J., et al.: The role of surface lattice defects of $CeO_{2-\delta}$ nanoparticles as a scavenging redox catalyst in polymer electrolyte membrane fuel cells. J. Mater. Chem. A **8**, 26023–26034 (2020). https://doi.org/10.1039/D0TA09397A
98. Baker, A.M., Stewart, S.M., Ramaiyan, K.P., et al.: Doped ceria nanoparticles with reduced solubility and improved peroxide decomposition activity for PEM fuel cells. J. Electrochem. Soc. **168**, 024507 (2021). https://doi.org/10.1149/1945-7111/abdee6
99. Singh, Y., White, R.T., Najm, M., et al.: Tracking the evolution of mechanical degradation in fuel cell membranes using 4D in situ visualization. J. Power Sources **412**, 224–237 (2019). https://doi.org/10.1016/j.jpowsour.2018.11.049
100. Jinnouchi, R., Kudo, K., Kodama, K., et al.: The role of oxygen-permeable ionomer for polymer electrolyte fuel cells. Nat. Commun. **12**, 4956 (2021). https://doi.org/10.1038/s41467-021-25301-3
101. Kodama, K., Motobayashi, K., Shinohara, A., et al.: Effect of the side-chain structure of perfluoro-sulfonic acid ionomers on the oxygen reduction reaction on the surface of Pt. ACS Catal. **8**, 694–700 (2018). https://doi.org/10.1021/acscatal.7b03571
102. Tang, M.H., Zhang, S.M., Chen, S.L.: Pt utilization in proton exchange membrane fuel cells: structure impacting factors and mechanistic insights. Chem. Soc. Rev. **51**, 1529–1546 (2022). https://doi.org/10.1039/d1cs00981h
103. Kodama, K., Shinohara, A., Hasegawa, N., et al.: Catalyst poisoning property of sulfonimide acid ionomer on Pt (111) surface. J. Electrochem. Soc. **161**, F649–F652 (2014). https://doi.org/10.1149/2.051405jes
104. Chowdhury, A., Bird, A., Liu, J.J., et al.: Linking perfluorosulfonic acid ionomer chemistry and high-current density performance in fuel-cell electrodes. ACS Appl. Mater. Interfaces **13**, 42579–42589 (2021). https://doi.org/10.1021/acsami.1c07611
105. International Renewable Energy Agency: Green hydrogen cost reduction: scaling up electrolysers to meet the 1.5 °C climate goal. https://www.irena.org/publications/2020/Dec/Green-hydrogen-cost-reduction (2020)
106. Kim, Y.S.: Polymer electrolytes with high ionic concentration for fuel cells and electrolyzers. ACS Appl. Polym. Mater. **3**, 1250–1270 (2021). https://doi.org/10.1021/acsapm.0c01405
107. Rolfi, A., Oldani, C., Merlo, L., et al.: New perfluorinated ionomer with improved oxygen permeability for application in cathode polymeric electrolyte membrane fuel cell. J. Power Sources **396**, 95–101 (2018). https://doi.org/10.1016/j.jpowsour.2018.05.093
108. Liu, Q.S., Lan, F.C., Chen, J.Q., et al.: A review of proton exchange membrane fuel cell water management: membrane electrode assembly. J. Power Sources **517**, 230723 (2022). https://doi.org/10.1016/j.jpowsour.2021.230723
109. Morgan, J.M., Datta, R.: Understanding the gas diffusion layer in proton exchange membrane fuel cells. I. How its structural characteristics affect diffusion and performance. J. Power Sources **251**, 269–278 (2014). https://doi.org/10.1016/j.jpowsour.2013.09.090
110. Omrani, R., Shabani, B.: Gas diffusion layer modifications and treatments for improving the performance of proton exchange membrane fuel cells and electrolysers: a review. Int. J. Hydrog. Energy **42**, 28515–28536 (2017). https://doi.org/10.1016/j.ijhydene.2017.09.132
111. Lee, F.C., Ismail, M.S., Ingham, D.B., et al.: Alternative architectures and materials for PEMFC gas diffusion layers: a review and outlook. Renew. Sustain. Energy Rev. **166**, 112640 (2022). https://doi.org/10.1016/j.rser.2022.112640
112. Ali Atyabi, S., Afshari, E.: Three-dimensional multiphase model of proton exchange membrane fuel cell with honeycomb flow field at the cathode side. J. Clean. Prod. **214**, 738–748 (2019). https://doi.org/10.1016/j.jclepro.2018.12.293
113. Park, J., Oh, H., Lee, Y.I., et al.: Effect of the pore size variation in the substrate of the gas diffusion layer on water management and fuel cell performance. Appl. Energy **171**, 200–212 (2016). https://doi.org/10.1016/j.apenergy.2016.02.132
114. Wu, H.W., Shih, G.J., Chen, Y.B.: Effect of operational parameters on transport and performance of a PEM fuel cell with the best protrusive gas diffusion layer arrangement. Appl. Energy **220**, 47–58 (2018). https://doi.org/10.1016/j.apenergy.2018.03.030
115. Barbir, F.: Main cell components, material properties, and processes. In: Barbir, F. (ed.) PEM Fuel Cells, pp. 73–117. Elsevier, Amsterdam (2013). https://doi.org/10.1016/b978-0-12-387710-9.00004-7
116. Jayakumar, A., Sethu, S.P., Ramos, M., et al.: A technical review on gas diffusion, mechanism and medium of PEM fuel cell. Ionics **21**, 1–18 (2015). https://doi.org/10.1007/s11581-014-1322-x
117. Li, H., Tang, Y.H., Wang, Z.W., et al.: A review of water flooding issues in the proton exchange membrane fuel cell. J. Power Sources **178**, 103–117 (2008). https://doi.org/10.1016/j.jpowsour.2007.12.068
118. Pasaogullari, U., Wang, C.Y.: Two-phase transport and the role of micro-porous layer in polymer electrolyte fuel cells. Electrochim. Acta **49**, 4359–4369 (2004). https://doi.org/10.1016/j.electacta.2004.04.027
119. Selamet, O.F., Pasaogullari, U., Spernjak, D., et al.: In situ two-phase flow investigation of proton exchange membrane (PEM) electrolyzer by simultaneous optical and neutron imaging. ECS Trans. **41**, 349–362 (2011). https://doi.org/10.1149/1.3635568
120. Moçotéguy, P., Ludwig, B., Yousfi Steiner, N.: Application of current steps and design of experiments methodology to the detection of water management faults in a proton exchange membrane fuel cell stack. J. Power Sources **303**, 126–136 (2016). https://doi.org/10.1016/j.jpowsour.2015.10.078
121. Shao, H., Qiu, D.K., Peng, L.F., et al.: In-situ measurement of temperature and humidity distribution in gas channels for commercial-size proton exchange membrane fuel cells. J. Power Sources **412**, 717–724 (2019). https://doi.org/10.1016/j.jpowsour.2018.12.008
122. Shao, H., Qiu, D.K., Peng, L.F., et al.: Modeling and analysis of water droplet dynamics in the dead-ended anode gas channel for proton exchange membrane fuel cells. Renew. Energy **138**, 842–851 (2019). https://doi.org/10.1016/j.renene.2019.02.028
123. Thampan, T., Malhotra, S., Tang, H., et al.: Modeling of conductive transport in proton-exchange membranes for fuel cells. J.

Electrochem. Soc. **147**, 3242 (2000). https://doi.org/10.1149/1.1393890
124. Holmström, N., Ihonen, J., Lundblad, A., et al.: The influence of the gas diffusion layer on water management in polymer electrolyte fuel cells. Fuel Cells **7**, 306–313 (2007). https://doi.org/10.1002/fuce.200700003
125. Nguyen, T.V.: Water management by material design and engineering for PEM fuel cells. ECS Trans. **3**, 1171–1180 (2006). https://doi.org/10.1149/1.2356236
126. Weber, A.Z., Newman, J.: Effects of microporous layers in polymer electrolyte fuel cells. J. Electrochem. Soc. **152**, A677 (2005). https://doi.org/10.1149/1.1861194
127. Atiyeh, H.K., Karan, K., Peppley, B., et al.: Experimental investigation of the role of a microporous layer on the water transport and performance of a PEM fuel cell. J. Power Sources **170**, 111–121 (2007). https://doi.org/10.1016/j.jpowsour.2007.04.016
128. Gostick, J.T., Ioannidis, M.A., Fowler, M.W., et al.: On the role of the microporous layer in PEMFC operation. Electrochem. Commun. **11**, 576–579 (2009). https://doi.org/10.1016/j.elecom.2008.12.053
129. Nam, J.H., Lee, K.J., Hwang, G.S., et al.: Microporous layer for water morphology control in PEMFC. Int. J. Heat Mass Transf. **52**, 2779–2791 (2009). https://doi.org/10.1016/j.ijheatmasstransfer.2009.01.002
130. Martinez, N., Peng, Z., Morin, A., et al.: Real time monitoring of water distribution in an operando fuel cell during transient states. J. Power Sources **365**, 230–234 (2017). https://doi.org/10.1016/j.jpowsour.2017.08.067
131. Tardy, E., Courtois, F., Chandesris, M., et al.: Investigation of liquid water heterogeneities in large area PEM fuel cells using a pseudo-3D multiphysics model. Int. J. Heat Mass Transf. **145**, 118720 (2019). https://doi.org/10.1016/j.ijheatmasstransfer.2019.118720
132. Ito, H., Ishikawa, T., Ishida, M., et al.: Measurement of net water drag coefficients in polymer electrolyte fuel cells under cathode-dry conditions. J. Electrochem. Soc. **166**, F1117–F1127 (2019). https://doi.org/10.1149/2.0051915jes
133. Gandomi, Y.A., Edmundson, M.D., Busby, F.C., et al.: Water management in polymer electrolyte fuel cells through asymmetric thermal and mass transport engineering of the micro-porous layers. J. Electrochem. Soc. **163**, F933–F944 (2016). https://doi.org/10.1149/2.1331608jes
134. Latorrata, S., Gallo Stampino, P., Cristiani, C., et al.: Novel superhydrophobic microporous layers for enhanced performance and efficient water management in PEM fuel cells. Int. J. Hydrog. Energy **39**, 5350–5357 (2014). https://doi.org/10.1016/j.ijhydene.2013.12.199
135. Öztürk, A., Fıçıcılar, B., Eroğlu, İ, et al.: Facilitation of water management in low Pt loaded PEM fuel cell by creating hydrophobic microporous layer with PTFE, FEP and PDMS polymers: effect of polymer and carbon amounts. Int. J. Hydrog. Energy **42**, 21226–21249 (2017). https://doi.org/10.1016/j.ijhydene.2017.06.202
136. Yu, S.C., Li, X.J., Hao, J.K., et al.: Preparation of microporous layer for proton exchange membrane fuel cell by using polyvinylpyrrolidone aqueous solution. Int. J. Hydrog. Energy **39**, 15681–15686 (2014). https://doi.org/10.1016/j.ijhydene.2014.07.062
137. Yan, W.M., Wu, D.K., Wang, X.D., et al.: Optimal microporous layer for proton exchange membrane fuel cell. J. Power Sources **195**, 5731–5734 (2010). https://doi.org/10.1016/j.jpowsour.2010.03.041
138. Ong, A.L., Bottino, A., Capannelli, G., et al.: Effect of preparative parameters on the characteristic of poly(vinylidene fluoride)-based microporous layer for proton exchange membrane fuel cells. J. Power Sources **183**, 62–68 (2008). https://doi.org/10.1016/j.jpowsour.2008.04.064
139. Kitahara, T., Nakajima, H., Inamoto, M., et al.: Influence of triple MPL coated GDL on the PEFC performance under low and high humidity. ECS Trans. **58**, 1401–1408 (2013). https://doi.org/10.1149/05801.1401ecst
140. Kitahara, T., Nakajima, H., Inamoto, M., et al.: Triple microporous layer coated gas diffusion layer for performance enhancement of polymer electrolyte fuel cells under both low and high humidity conditions. J. Power Sources **248**, 1256–1263 (2014). https://doi.org/10.1016/j.jpowsour.2013.10.066
141. Chun, J.H., Park, K.T., Jo, D.H., et al.: Development of a novel hydrophobic/hydrophilic double micro porous layer for use in a cathode gas diffusion layer in PEMFC. Int. J. Hydrog. Energy **36**, 8422–8428 (2011). https://doi.org/10.1016/j.ijhydene.2011.04.038
142. Kitahara, T., Nakajima, H., Mori, K.: Hydrophilic and hydrophobic double microporous layer coated gas diffusion layer for enhancing performance of polymer electrolyte fuel cells under no-humidification at the cathode. J. Power Sources **199**, 29–36 (2012). https://doi.org/10.1016/j.jpowsour.2011.10.002
143. Kitahara, T., Nakajima, H., Inamoto, M., et al.: Novel hydrophilic and hydrophobic double microporous layer coated gas diffusion layer to enhance performance of polymer electrolyte fuel cells under both low and high humidity. J. Power Sources **234**, 129–138 (2013). https://doi.org/10.1016/j.jpowsour.2013.01.150
144. Wu, R., Zhu, X., Liao, Q., et al.: Liquid and oxygen transport in defective bilayer gas diffusion material of proton exchange membrane fuel cell. Int. J. Hydrog. Energy **38**, 4067–4078 (2013). https://doi.org/10.1016/j.ijhydene.2013.01.045
145. Sasabe, T., Deevanhxay, P., Tsushima, S., et al.: Soft X-ray visualization of the liquid water transport within the cracks of micro porous layer in PEMFC. Electrochem. Commun. **13**, 638–641 (2011). https://doi.org/10.1016/j.elecom.2011.03.033
146. Markötter, H., Haußmann, J., Alink, R., et al.: Influence of cracks in the microporous layer on the water distribution in a PEM fuel cell investigated by synchrotron radiography. Electrochem. Commun. **34**, 22–24 (2013). https://doi.org/10.1016/j.elecom.2013.04.006
147. Deevanhxay, P., Sasabe, T., Tsushima, S., et al.: Effect of liquid water distribution in gas diffusion media with and without microporous layer on PEM fuel cell performance. Electrochem. Commun. **34**, 239–241 (2013). https://doi.org/10.1016/j.elecom.2013.07.001
148. Wargo, E.A., Schulz, V.P., Çeçen, A., et al.: Resolving macro- and micro-porous layer interaction in polymer electrolyte fuel cells using focused ion beam and X-ray computed tomography. Electrochim. Acta **87**, 201–212 (2013). https://doi.org/10.1016/j.electacta.2012.09.008
149. Ma, J.S., Zhang, X.X., Jiang, Z., et al.: Flow properties of an intact MPL from nano-tomography and pore network modelling. Fuel **136**, 307–315 (2014). https://doi.org/10.1016/j.fuel.2014.07.040
150. Okuhata, G., Tonoike, T., Nishida, K., et al.: Effect of perforation structure of cathode GDL on liquid water removal in PEFC. ECS Trans. **58**, 1047–1057 (2013). https://doi.org/10.1149/05801.1047ecst
151. Lu, Z.J., Waldecker, J., Xie, X.B., et al.: Investigation of water transport in perforated gas diffusion layer by neutron radiography. ECS Trans. **58**, 315–324 (2013). https://doi.org/10.1149/05801.0315ecst
152. Markötter, H., Alink, R., Haußmann, J., et al.: Visualization of the water distribution in perforated gas diffusion layers by means of synchrotron X-ray radiography. Int. J. Hydrog. Energy **37**, 7757–7761 (2012). https://doi.org/10.1016/j.ijhydene.2012.01.141

153. Gerteisen, D., Sadeler, C.: Stability and performance improvement of a polymer electrolyte membrane fuel cell stack by laser perforation of gas diffusion layers. J. Power Sources **195**, 5252–5257 (2010). https://doi.org/10.1016/j.jpowsour.2010.03.021
154. Manahan, M.P., Clement, J.T., Srouji, A.K., et al.: Laser modified fuel cell diffusion media: engineering enhanced performance via localized water redistribution. J. Electrochem. Soc. **161**, F1061–F1069 (2014). https://doi.org/10.1149/2.0591410jes
155. Haußmann, J., Markötter, H., Alink, R., et al.: Synchrotron radiography and tomography of water transport in perforated gas diffusion media. J. Power Sources **239**, 611–622 (2013). https://doi.org/10.1016/j.jpowsour.2013.02.014
156. Manahan, M., Mench, M.: Increased performance of PEFCs with engineered mass-transport pathways. ECS Trans. **41**, 569–581 (2011). https://doi.org/10.1149/1.3635590
157. Manahan, M.P., Hatzell, M.C., Kumbur, E.C., et al.: Laser perforated fuel cell diffusion media. Part I: related changes in performance and water content. J. Power Sources **196**, 5573–5582 (2011). https://doi.org/10.1016/j.jpowsour.2011.01.014
158. Alink, R., Haußmann, J., Markötter, H., et al.: The influence of porous transport layer modifications on the water management in polymer electrolyte membrane fuel cells. J. Power Sources **233**, 358–368 (2013). https://doi.org/10.1016/j.jpowsour.2013.01.085
159. Wang, D.L., Xin, H.L., Hovden, R., et al.: Structurally ordered intermetallic platinum–cobalt core–shell nanoparticles with enhanced activity and stability as oxygen reduction electrocatalysts. Nat. Mater. **12**, 81–87 (2013). https://doi.org/10.1038/nmat3458
160. Liu, M.L., Zhao, Z.P., Duan, X.F., et al.: Nanoscale structure design for high-performance Pt-based ORR catalysts. Adv. Mater. **31**, 1802234 (2019). https://doi.org/10.1002/adma.201802234
161. Peron, J., Mani, A.N., Zhao, X.S., et al.: Properties of Nafion® NR-211 membranes for PEMFCs. J. Membr. Sci. **356**, 44–51 (2010). https://doi.org/10.1016/j.memsci.2010.03.025
162. Guccini, V., Carlson, A., Yu, S., et al.: Highly proton conductive membranes based on carboxylated cellulose nanofibres and their performance in proton exchange membrane fuel cells. J. Mater. Chem. A **7**, 25032–25039 (2019). https://doi.org/10.1039/C9TA04898G
163. Li, G.B., Zhao, C.J., Li, X.F., et al.: Novel side-chain-type sulfonated diphenyl-based poly(arylene ether sulfone)s with a hydrogen-bonded network as proton exchange membranes. Polym. Chem. **6**, 5911–5920 (2015). https://doi.org/10.1039/c5py00700c
164. Ozden, A., Shahgaldi, S., Li, X.G., et al.: A review of gas diffusion layers for proton exchange membrane fuel cells: with a focus on characteristics, characterization techniques, materials and designs. Prog. Energy Combust. Sci. **74**, 50–102 (2019). https://doi.org/10.1016/j.pecs.2019.05.002
165. Wang, M., Park, J.H., Kabir, S., et al.: Impact of catalyst ink dispersing methodology on fuel cell performance using in situ X-ray scattering. ACS Appl. Energy Mater. **2**, 6417–6427 (2019). https://doi.org/10.1021/acsaem.9b01037
166. Bapat, S., Giehl, C., Kohsakowski, S., et al.: On the state and stability of fuel cell catalyst inks. Adv. Powder Technol. **32**, 3845–3859 (2021). https://doi.org/10.1016/j.apt.2021.08.030
167. Du, S.J., Li, W.K., Wu, H., et al.: Effects of ionomer and dispersion methods on rheological behavior of proton exchange membrane fuel cell catalyst layer ink. Int. J. Hydrog. Energy **45**, 29430–29441 (2020). https://doi.org/10.1016/j.ijhydene.2020.07.241
168. Li, B., Liu, Y., Guo, Y.Q., et al.: Controlling the microscopic morphology and permeability of catalyst layers in proton exchange membrane fuel cells by adjusting catalyst ink agglomerates. Int. J. Hydrog. Energy **46**, 32215–32225 (2021). https://doi.org/10.1016/j.ijhydene.2021.06.216
169. Yang, D.Z., Guo, Y.Q., Tang, H.F., et al.: Effect of rheological properties of catalyst slurry on the structure of catalyst layer in PEMFC. Int. J. Hydrog. Energy **47**, 8956–8964 (2022). https://doi.org/10.1016/j.ijhydene.2021.12.227
170. Jie, N.: Investigation of the colloidal behaviour of carbon black and perfluorosulfonated ionomer in various solvents. Dissertation, Queen's University (2016). http://hdl.handle.net/1974/14081.
171. So, S., Kang, H., Choi, D., et al.: Tunable aggregation of short-side-chain perfluorinated sulfonic acid ionomers for the catalyst layer in polymer electrolyte membrane fuel cells. Int. J. Hydrog. Energy **45**, 19891–19899 (2020). https://doi.org/10.1016/j.ijhydene.2020.05.128
172. Lei, C., Yang, F., MacAuley, N., et al.: Impact of catalyst ink dispersing solvent on PEM fuel cell performance and durability. J. Electrochem. Soc. **168**, 044517 (2021). https://doi.org/10.1149/1945-7111/abf2b0
173. Sharma, R., Andersen, S.M.: Zoom in catalyst/ionomer interface in polymer electrolyte membrane fuel cell electrodes: impact of catalyst/ionomer dispersion media/solvent. ACS Appl. Mater. Interfaces **10**, 38125–38133 (2018). https://doi.org/10.1021/acsami.8b14622
174. So, M., Ohnishi, T., Park, K., et al.: The effect of solvent and ionomer on agglomeration in fuel cell catalyst inks: simulation by the discrete element method. Int. J. Hydrog. Energy **44**, 28984–28995 (2019). https://doi.org/10.1016/j.ijhydene.2019.09.012
175. Fernández, R., Ferreira-Aparicio, P., Daza, L.: PEMFC electrode preparation: influence of the solvent composition and evaporation rate on the catalytic layer microstructure. J. Power Sources **151**, 18–24 (2005). https://doi.org/10.1016/j.jpowsour.2005.02.048
176. Khandavalli, S., Park, J.H., Kariuki, N.N., et al.: Rheological investigation on the microstructure of fuel cell catalyst inks. ACS Appl. Mater. Interfaces **10**, 43610–43622 (2018). https://doi.org/10.1021/acsami.8b15039
177. Gong, Q., Li, C.Z., Liu, Y.D., et al.: Effects of ink formulation on construction of catalyst layers for high-performance polymer electrolyte membrane fuel cells. ACS Appl. Mater. Interfaces **13**, 37004–37013 (2021). https://doi.org/10.1021/acsami.1c06711
178. Sabli, N., Abu Bakar, N.A., Izhar, S., et al.: Membrane electrode assembly with high efficiency and stability: effect of solvent type and membrane composition. Sains Malays. **48**, 877–885 (2019). https://doi.org/10.17576/jsm-2019-4804-20
179. Balu, R., Choudhury, N.R., Mata, J.P., et al.: Evolution of the interfacial structure of a catalyst ink with the quality of the dispersing solvent: a contrast variation small-angle and ultrasmall-angle neutron scattering investigation. ACS Appl. Mater. Interfaces **11**, 9934–9946 (2019). https://doi.org/10.1021/acsami.8b20645
180. Guo, Y.Q., Yang, D.Z., Li, B., et al.: Effect of dispersion solvents and ionomers on the rheology of catalyst inks and catalyst layer structure for proton exchange membrane fuel cells. ACS Appl. Mater. Interfaces **13**, 27119–27128 (2021). https://doi.org/10.1021/acsami.1c07070
181. Gatto, I., Saccà, A., Sebastián, D., et al.: Influence of ionomer content in the catalytic layer of MEAs based on Aquivion® ionomer. Polymers **13**, 3832 (2021). https://doi.org/10.3390/polym13213832
182. Sasikumar, G., Ihm, J.W., Ryu, H.: Optimum Nafion content in PEM fuel cell electrodes. Electrochim. Acta **50**, 601–605 (2004). https://doi.org/10.1016/j.electacta.2004.01.126

183. Shen, S.Y., Han, A.D., Yan, X.H., et al.: Influence of equivalent weight of ionomer on proton conduction behavior in fuel cell catalyst layers. J. Electrochem. Soc. **166**, F724–F728 (2019)
184. Myers, D.J., Kropf, A.J., Wegener, E.C., et al.: Degradation of platinum–cobalt alloy PEMFC cathode catalysts in catalyst-ionomer inks. J. Electrochem. Soc. **168**, 044510 (2021). https://doi.org/10.1149/1945-7111/abf4ab
185. Yang, F., Xin, L., Uzunoglu, A., et al.: Investigation of the interaction between nafion ionomer and surface functionalized carbon black using both ultrasmall angle X-ray scattering and cryo-TEM. ACS Appl. Mater. Interfaces **9**, 6530–6538 (2017). https://doi.org/10.1021/acsami.6b12949
186. Orfanidi, A., Madkikar, P., El-Sayed, H.A., et al.: The key to high performance low Pt loaded electrodes. J. Electrochem. Soc. **164**, F418–F426 (2017). https://doi.org/10.1149/2.1621704jes
187. Ott, S., Orfanidi, A., Schmies, H., et al.: Ionomer distribution control in porous carbon-supported catalyst layers for high-power and low Pt-loaded proton exchange membrane fuel cells. Nat. Mater. **19**, 77–85 (2020). https://doi.org/10.1038/s41563-019-0487-0
188. Yoshimune, W., Harada, M.: Temperature-induced shear-thinning in catalyst inks. Electrochem. Commun. **130**, 107099 (2021). https://doi.org/10.1016/j.elecom.2021.107099
189. Shukla, S., Bhattacharjee, S., Weber, A.Z., et al.: Experimental and theoretical analysis of ink dispersion stability for polymer electrolyte fuel cell applications. J. Electrochem. Soc. **164**, F600–F609 (2017). https://doi.org/10.1149/2.0961706jes
190. Uemura, S., Kameya, Y., Iriguchi, N., et al.: Communication: investigation of catalyst ink degradation by X-ray CT. J. Electrochem. Soc. **165**, F142–F144 (2018). https://doi.org/10.1149/2.0411803jes
191. Lim, B.H., Majlan, E.H., Tajuddin, A., et al.: Comparison of catalyst-coated membranes and catalyst-coated substrate for PEMFC membrane electrode assembly: a review. Chin. J. Chem. Eng. **33**, 1–16 (2021). https://doi.org/10.1016/j.cjche.2020.07.044
192. Tang, H.L., Wang, S.L., Jiang, S.P., et al.: A comparative study of CCM and hot-pressed MEAs for PEM fuel cells. J. Power Sources **170**, 140–144 (2007). https://doi.org/10.1016/j.jpowsour.2007.03.062
193. Mauger, S.A., Wang, M., Cetinbas, F.C., et al.: Development of high-performance roll-to-roll-coated gas-diffusion-electrode-based fuel cells. J. Power Sources **506**, 230039 (2021). https://doi.org/10.1016/j.jpowsour.2021.230039
194. Hasegawa, N., Kamiya, A., Matsunaga, T., et al.: Analysis of crack formation during fuel cell catalyst ink drying process. Reduction of catalyst layer cracking by addition of high boiling point solvent. Colloids Surf. A Physicochem. Eng. Aspects **628**, 127153 (2021). https://doi.org/10.1016/j.colsurfa.2021.127153
195. Stähler, M., Stähler, A., Scheepers, F., et al.: A completely slot die coated membrane electrode assembly. Int. J. Hydrog. Energy **44**, 7053–7058 (2019). https://doi.org/10.1016/j.ijhydene.2019.02.016
196. Arcot, M.P., Zheng, K., McGrory, J., et al.: Investigation of catalyst layer defects in catalyst-coated membrane for PEMFC application: non-destructive method. Int. J. Energy Res. **42**, 3615–3632 (2018). https://doi.org/10.1002/er.4107
197. Talukdar, K., Helmly, S., Schulze, M., et al.: Enveloping of catalyst powder by ionomer for dry spray coating in polymer electrolyte membrane fuel cells. J. Power Sources **424**, 82–90 (2019). https://doi.org/10.1016/j.jpowsour.2019.03.093
198. Waldrop, K., Wycisk, R., Pintauro, P.N.: Application of electrospinning for the fabrication of proton-exchange membrane fuel cell electrodes. Curr. Opin. Electrochem. **21**, 257–264 (2020). https://doi.org/10.1016/j.coelec.2020.03.007
199. Hwang, D.S., Park, C.H., Yi, S.C., et al.: Optimal catalyst layer structure of polymer electrolyte membrane fuel cell. Int. J. Hydrog. Energy **36**, 9876–9885 (2011). https://doi.org/10.1016/j.ijhydene.2011.05.073
200. Mehta, V., Cooper, J.S.: Review and analysis of PEM fuel cell design and manufacturing. J. Power Sources **114**, 32–53 (2003). https://doi.org/10.1016/S0378-7753(02)00542-6
201. Bodner, M., García, H.R., Steenberg, T., et al.: Enabling industrial production of electrodes by use of slot-die coating for HT-PEM fuel cells. Int. J. Hydrog. Energy **44**, 12793–12801 (2019). https://doi.org/10.1016/j.ijhydene.2018.11.091
202. Creel, E.B., Tjiptowidjojo, K., Lee, J.A., et al.: Slot-die-coating operability windows for polymer electrolyte membrane fuel cell cathode catalyst layers. J. Colloid Interface Sci. **610**, 474–485 (2022). https://doi.org/10.1016/j.jcis.2021.11.047
203. Park, J., Shin, K., Lee, C.: Roll-to-roll coating technology and its applications: a review. Int. J. Precis. Eng. Manuf. **17**, 537–550 (2016). https://doi.org/10.1007/s12541-016-0067-z
204. Sun, Y.Y., Polani, S., Luo, F., et al.: Advancements in cathode catalyst and cathode layer design for proton exchange membrane fuel cells. Nat. Commun. **12**, 5984 (2021). https://doi.org/10.1038/s41467-021-25911-x
205. Dixit, M.B., Harkey, B.A., Shen, F.Y., et al.: Catalyst layer ink interactions that affect coatability. J. Electrochem. Soc. **165**, F264–F271 (2018). https://doi.org/10.1149/2.0191805jes
206. Glüsen, A., Müller, M., Stolten, D.: Slot-die coating: a new preparation method for direct methanol fuel cells catalyst layers. J. Fuel Cell Sci. Technol. **10**, 044503 (2013). https://doi.org/10.1115/1.4024607
207. Kim, S.M., Ahn, C.Y., Cho, Y.H., et al.: High-performance fuel cell with stretched catalyst-coated membrane: one-step formation of cracked electrode. Sci. Rep. **6**, 26503 (2016). https://doi.org/10.1038/srep26503
208. Tsushima, S., Hirai, S.: An overview of cracks and interfacial voids in membrane electrode assemblies in polymer electrolyte fuel cells. J. Therm. Sci. Technol. **10**, JTST0002 (2015). https://doi.org/10.1299/jtst.2015jtst0002
209. Zhang, Z.S., Sadeghi, M.A., Jervis, R., et al.: Tailoring carbon nanotube microsphere architectures with controlled porosity. Adv. Funct. Mater. **29**, 1903983 (2019). https://doi.org/10.1002/adfm.201903983
210. Suzuki, T., Tanaka, H., Hayase, M., et al.: Investigation of porous structure formation of catalyst layers for proton exchange membrane fuel cells and their effect on cell performance. Int. J. Hydrog. Energy **41**, 20326–20335 (2016). https://doi.org/10.1016/j.ijhydene.2016.09.078
211. Koga, M., Matsumoto, H., Tokita, M., et al.: Investigation of drying process of catalyst ink for polymer electrolyte fuel cells by grazing-incidence X-ray scattering. ECS Trans. **86**, 157–161 (2018). https://doi.org/10.1149/08613.0157ecst
212. Park, H.S., Cho, Y.H., Cho, Y.H., et al.: Performance enhancement of PEMFC through temperature control in catalyst layer fabrication. Electrochim. Acta **53**, 763–767 (2007). https://doi.org/10.1016/j.electacta.2007.07.046
213. Komoda, Y., Okabayashi, K., Nishimura, H., et al.: Dependence of polymer electrolyte fuel cell performance on preparation conditions of slurry for catalyst layers. J. Power Sources **193**, 488–494 (2009). https://doi.org/10.1016/j.jpowsour.2009.04.015
214. Talukdar, K., Delgado, S., Lagarteira, T., et al.: Minimizing mass-transport loss in proton exchange membrane fuel cell by freeze-drying of cathode catalyst layers. J. Power Sources **427**, 309–317 (2019). https://doi.org/10.1016/j.jpowsour.2019.04.094
215. Chen, G.H., Wang, W.: Role of freeze drying in nanotechnology. Dry. Technol. **25**, 29–35 (2007). https://doi.org/10.1080/07373930601161179

216. Talukdar, K., Ripan, M.A., Jahnke, T., et al.: Experimental and numerical study on catalyst layer of polymer electrolyte membrane fuel cell prepared with diverse drying methods. J. Power Sources **461**, 228169 (2020). https://doi.org/10.1016/j.jpowsour.2020.228169
217. Kusano, T., Hiroi, T., Amemiya, K., et al.: Structural evolution of a catalyst ink for fuel cells during the drying process investigated by CV-SANS. Polym. J. **47**, 546–555 (2015). https://doi.org/10.1038/pj.2015.36
218. Phillips, A., Ulsh, M., Neyerlin, K.C., et al.: Impacts of electrode coating irregularities on polymer electrolyte membrane fuel cell lifetime using quasi in situ infrared thermography and accelerated stress testing. Int. J. Hydrog. Energy **43**, 6390–6399 (2018). https://doi.org/10.1016/j.ijhydene.2018.02.050
219. Wang, M., Rome, G., Medina, S., et al.: Impact of electrode thick spot irregularities on polymer electrolyte membrane fuel cell initial performance. J. Power Sources **466**, 228344 (2020). https://doi.org/10.1016/j.jpowsour.2020.228344
220. Garsany, Y., Atkinson, R.W., Gould, B.D., et al.: Dual-layer catalyst layers for increased proton exchange membrane fuel cell performance. J. Power Sources **514**, 230574 (2021). https://doi.org/10.1016/j.jpowsour.2021.230574
221. Bayrakçeken, A., Erkan, S., Türker, L., et al.: Effects of membrane electrode assembly components on proton exchange membrane fuel cell performance. Int. J. Hydrog. Energy **33**, 165–170 (2008). https://doi.org/10.1016/j.ijhydene.2007.08.021
222. Yurko, Y., Elbaz, L.: The effect of membrane electrode assembly methods on the performance in fuel cells. Electrochim. Acta **389**, 138676 (2021). https://doi.org/10.1016/j.electacta.2021.138676
223. Bazylak, A., Sinton, D., Liu, Z.S., et al.: Effect of compression on liquid water transport and microstructure of PEMFC gas diffusion layers. J. Power Sources **163**, 784–792 (2007). https://doi.org/10.1016/j.jpowsour.2006.09.045
224. Park, T., Chang, I., Jung, J.H., et al.: Effect of assembly pressure on the performance of a bendable polymer electrolyte fuel cell based on a silver nanowire current collector. Energy **134**, 412–419 (2017). https://doi.org/10.1016/j.energy.2017.05.197
225. Satterfield, M.B., Majsztrik, P.W., Ota, H., et al.: Mechanical properties of Nafion and titania/Nafion composite membranes for polymer electrolyte membrane fuel cells. J. Polym. Sci. B Polym. Phys. **44**, 2327–2345 (2006). https://doi.org/10.1002/polb.20857
226. Therdthianwong, A., Manomayidthikarn, P., Therdthianwong, S.: Investigation of membrane electrode assembly (MEA) hot-pressing parameters for proton exchange membrane fuel cell. Energy **32**, 2401–2411 (2007). https://doi.org/10.1016/j.energy.2007.07.005
227. Nakrumpai, B., Pruksathorn, K., Piumsomboon, P.: Optimum condition of membrane electrode assembly fabrication for PEM fuel cells. Korean J. Chem. Eng. **23**, 570–575 (2006). https://doi.org/10.1007/BF02706796
228. Hack, J., Heenan, T.M.M., Iacoviello, F., et al.: A structure and durability comparison of membrane electrode assembly fabrication methods: self-assembled versus hot-pressed. J. Electrochem. Soc. **165**, F3045–F3052 (2018). https://doi.org/10.1149/2.0051806jes
229. Alizadeh, E., Ghadimi, M., Barzegari, M.M., et al.: Development of contact pressure distribution of PEM fuel cell's MEA using novel clamping mechanism. Energy **131**, 92–97 (2017). https://doi.org/10.1016/j.energy.2017.05.036
230. Debe, M.K.: Electrocatalyst approaches and challenges for automotive fuel cells. Nature **486**, 43–51 (2012). https://doi.org/10.1038/nature11115
231. Chen, J.K., Liu, H.M., Huang, Y., et al.: High-rate roll-to-roll stack and lamination of multilayer structured membrane electrode assembly. J. Manuf. Process. **23**, 175–182 (2016). https://doi.org/10.1016/j.jmapro.2016.06.022
232. Chen, J.K., Jiang, X., Tang, W., et al.: Roll-to-roll stack and lamination of gas diffusion layer in multilayer structured membrane electrode assembly. Proc Inst. Mech. Eng. B J. Eng. Manuf. **234**, 66–74 (2020). https://doi.org/10.1177/0954405419862090
233. Devaraj, V., Lopez, L.F., Beaman, J.J., et al.: Model-based control of a continuous coating line for proton exchange membrane fuel cell electrode assembly. Int. J. Chem. Eng. **2015**, 1–11 (2015). https://doi.org/10.1155/2015/572983
234. Weidner, J., Sethuraman, V., Zee, J.V.: Engineering a membrane electrode assembly. Electrochem. Soc. Interface **12**, 40–43 (2003)
235. Sui, S., Wang, X.Y., Zhou, X.T., et al.: A comprehensive review of Pt electrocatalysts for the oxygen reduction reaction: nanostructure, activity, mechanism and carbon support in PEM fuel cells. J. Mater. Chem. A **5**, 1808–1825 (2017). https://doi.org/10.1039/C6TA08580F
236. Banham, D., Ye, S.Y.: Current status and future development of catalyst materials and catalyst layers for proton exchange membrane fuel cells: an industrial perspective. ACS Energy Lett. **2**, 629–638 (2017). https://doi.org/10.1021/acsenergylett.6b00644
237. Zhang, L., Zhao, Y., Banis, M.N., et al.: Rational design of porous structures via molecular layer deposition as an effective stabilizer for enhancing Pt ORR performance. Nano Energy **60**, 111–118 (2019). https://doi.org/10.1016/j.nanoen.2019.03.033
238. Banham, D., Choi, J.Y., Kishimoto, T., et al.: Integrating PGM-free catalysts into catalyst layers and proton exchange membrane fuel cell devices. Adv. Mater. **31**, 1804846 (2019). https://doi.org/10.1002/adma.201804846
239. Geng, D.S., Chen, Y., Chen, Y.G., et al.: High oxygen-reduction activity and durability of nitrogen-doped graphene. Energy Environ. Sci. **4**, 760–764 (2011). https://doi.org/10.1039/C0EE00326C
240. Banham, D., Kishimoto, T., Zhou, Y.J., et al.: Critical advancements in achieving high power and stable nonprecious metal catalyst-based MEAs for real-world proton exchange membrane fuel cell applications. Sci. Adv. **4**, eaar7180 (2018). https://doi.org/10.1126/sciadv.aar7180
241. Choi, J.Y., Yang, L.J., Kishimoto, T., et al.: Is the rapid initial performance loss of Fe/N/C non precious metal catalysts due to micropore flooding? Energy Environ. Sci. **10**, 296–305 (2017). https://doi.org/10.1039/C6EE03005J
242. Guan, S.M., Zhou, F., Du, S.J., et al.: Optimization of the interface between catalyst layer and proton exchange membrane via rolled technique. J. Electrochem. Soc. **169**, 014504 (2022). https://doi.org/10.1149/1945-7111/ac44bd
243. Ahn, C.Y., Jang, S., Cho, Y.H., et al.: Guided cracking of electrodes by stretching prism-patterned membrane electrode assemblies for high-performance fuel cells. Sci. Rep. **8**, 1257 (2018). https://doi.org/10.1038/s41598-018-19861-6
244. Shin, S.J., Lee, J.K., Ha, H.Y., et al.: Effect of the catalytic ink preparation method on the performance of polymer electrolyte membrane fuel cells. J. Power Sources **106**, 146–152 (2002). https://doi.org/10.1016/s0378-7753(01)01045-x
245. Holdcroft, S.: Fuel cell catalyst layers: a polymer science perspective. Chem. Mater. **26**, 381–393 (2014). https://doi.org/10.1021/cm401445h
246. Zhao, N.N., Shi, Z.Q., Girard, F.: Superior proton exchange membrane fuel cell (PEMFC) performance using short-side-chain perfluorosulfonic acid (PFSA) membrane and ionomer. Materials **15**, 78 (2022). https://doi.org/10.3390/ma15010078
247. Ren, H., Meng, X.C., Lin, Y.L., et al.: Structural stability of catalyst ink and its effects on the catalyst layer microstructure and fuel cell performance. J. Power Sources **517**, 230698 (2022). https://doi.org/10.1016/j.jpowsour.2021.230698

248. Fraser, A., Zhang, Z.S., Merle, G., et al.: Composite carbon nanotube microsphere coatings for use as electrode supports. Adv. Funct. Mater. **28**, 1803713 (2018). https://doi.org/10.1002/adfm.201803713
249. Yang, T.F., Hourng, L.W., Yu, T.L., et al.: High performance proton exchange membrane fuel cell electrode assemblies. J. Power Sources **195**, 7359–7369 (2010). https://doi.org/10.1016/j.jpowsour.2010.04.063
250. Xia, Z.X., Wang, S.L., Jiang, L.H., et al.: Controllable synthesis of vertically aligned polypyrrole nanowires as advanced electrode support for fuel cells. J. Power Sources **256**, 125–132 (2014). https://doi.org/10.1016/j.jpowsour.2013.12.013
251. Hsieh, Y.C., Zhang, Y., Su, D., et al.: Ordered bilayer ruthenium–platinum core–shell nanoparticles as carbon monoxide-tolerant fuel cell catalysts. Nat. Commun. **4**, 1–9 (2013). https://doi.org/10.1038/ncomms3466
252. Du, C.Y., Cheng, X.Q., Yang, T., et al.: Numerical simulation of the ordered catalyst layer in cathode of proton exchange membrane fuel cells. Electrochem. Commun. **7**, 1411–1416 (2005). https://doi.org/10.1016/j.elecom.2005.09.022
253. Du, C.Y., Yang, T., Shi, P.F., et al.: Performance analysis of the ordered and the conventional catalyst layers in proton exchange membrane fuel cells. Electrochim. Acta **51**, 4934–4941 (2006). https://doi.org/10.1016/j.electacta.2006.01.047
254. Hussain, M.M., Song, D., Liu, Z.S., et al.: Modeling an ordered nanostructured cathode catalyst layer for proton exchange membrane fuel cells. J. Power Sources **196**, 4533–4544 (2011). https://doi.org/10.1016/j.jpowsour.2010.10.111
255. Middelman, E.: Improved PEM fuel cell electrodes by controlled self-assembly. Fuel Cells Bull. **2002**, 9–12 (2002). https://doi.org/10.1016/S1464-2859(02)11028-5
256. Deng, R.Y., Xia, Z.X., Sun, R.L., et al.: Nanostructured ultrathin catalyst layer with ordered platinum nanotube arrays for polymer electrolyte membrane fuel cells. J. Energy Chem. **43**, 33–39 (2020). https://doi.org/10.1016/j.jechem.2019.07.015
257. Aizawa, M., Gyoten, H., Salah, A., et al.: Pillar structured membranes for suppressing cathodic concentration overvoltage in PEMFCs at elevated temperature/low relative humidity. J. Electrochem. Soc. **157**, B1844 (2010). https://doi.org/10.1149/1.3502613
258. Kim, S.M., Kang, Y.S., Ahn, C., et al.: Prism-patterned Nafion membrane for enhanced water transport in polymer electrolyte membrane fuel cell. J. Power Sources **317**, 19–24 (2016). https://doi.org/10.1016/j.jpowsour.2016.03.083
259. Ning, F.D., Bai, C., Qin, J.Q., et al.: Great improvement in the performance and lifetime of a fuel cell using a highly dense, well-ordered, and cone-shaped Nafion array. J. Mater. Chem. A **8**, 5489–5500 (2020). https://doi.org/10.1039/C9TA13666E
260. Li, X.A., Forouzandeh, F., Fürstenhaupt, T., et al.: New insights into the surface properties of hard-templated ordered mesoporous carbons. Carbon **127**, 707–717 (2018). https://doi.org/10.1016/j.carbon.2017.11.049
261. Jiang, S.F., Yi, B.L., Zhang, C.K., et al.: Vertically aligned carbon-coated titanium dioxide nanorod arrays on carbon paper with low platinum for proton exchange membrane fuel cells. J. Power Sources **276**, 80–88 (2015). https://doi.org/10.1016/j.jpowsour.2014.11.093
262. Zhang, C.K., Yu, H.M., Li, Y.K., et al.: Supported noble metals on hydrogen-treated TiO_2 nanotube arrays as highly ordered electrodes for fuel cells. Chemsuschem **6**, 659–666 (2013). https://doi.org/10.1002/cssc.201200828
263. Zhang, C.K., Yu, H.M., Li, Y.K., et al.: Highly stable ternary tin–palladium–platinum catalysts supported on hydrogenated TiO_2 nanotube arrays for fuel cells. Nanoscale **5**, 6834–6841 (2013). https://doi.org/10.1039/c3nr01086d
264. Debe, M.K.: Tutorial on the fundamental characteristics and practical properties of nanostructured thin film (NSTF) catalysts. J. Electrochem. Soc. **160**, F522–F534 (2013). https://doi.org/10.1149/2.049306jes
265. Debe, M.K.: Novel catalysts, catalysts support and catalysts coated membrane methods. In: Vielstich, W., Gasteiger, H.A., Lamm, A., et al. (eds.) Handbook of Fuel Cells: Fundamentals, Technology and Applications, pp. 1–14 (2010). https://doi.org/10.1002/9780470974001.f303050
266. Jiang, S.F., Yi, B.L., Cao, L.S., et al.: Development of advanced catalytic layer based on vertically aligned conductive polymer arrays for thin-film fuel cell electrodes. J. Power Sources **329**, 347–354 (2016). https://doi.org/10.1016/j.jpowsour.2016.08.098
267. Wan, C.H., Lin, M.T., Zhuang, Q.H., et al.: Preparation and performance of novel MEA with multi catalyst layer structure for PEFC by magnetron sputter deposition technique. Surf. Coat. Technol. **201**, 214–222 (2006). https://doi.org/10.1016/j.surfcoat.2005.11.119
268. Gu, M.S., Kim, B.S.: Electrochemistry of multilayer electrodes: from the basics to energy applications. Acc. Chem. Res. **54**, 57–69 (2021). https://doi.org/10.1021/acs.accounts.0c00524
269. Shahgaldi, S., Ozden, A., Li, X.G., et al.: Cathode catalyst layer design with gradients of ionomer distribution for proton exchange membrane fuel cells. Energy Convers. Manag. **171**, 1476–1486 (2018). https://doi.org/10.1016/j.enconman.2018.06.078
270. Su, H.N., Zeng, Q., Liao, S.J., et al.: High performance membrane electrode assembly with ultra-low platinum loading prepared by a novel multi catalyst layer technique. Int. J. Hydrog. Energy **35**, 10430–10436 (2010). https://doi.org/10.1016/j.ijhydene.2010.06.070

Shanyun Mo is currently a master student at Guangzhou University. She received her undergraduate degree from North University of China. In 2019, She joined the research and development department of SinoHyKey Technology Company Ltd. Her research mainly focuses on proton exchange membrane modification, failure analysis of proton exchange membrane, and ionomer in the catalyst layer.

Lei Du is an Associate Professor at Guangzhou University. Before moving to Guangzhou, he was a postdoctoral fellow at Institut National de la Recherche Scientifique (Canada) and a lecturer at Harbin Institute of Technology (China). He received Ph.D. degree in 2017 from Harbin Institute of Technology. He also studied at Pacific Northwest National Laboratory and Washington State University as a visiting student during his Ph.D. period. His main research

interests include electrocatalysis in energy conversion and storage—new materials and new mechanisms, electrochemical device integration.

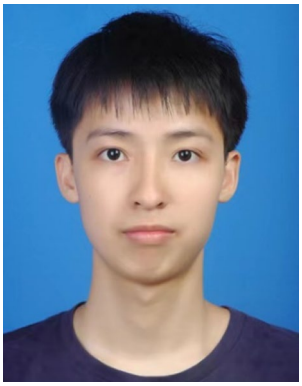

Zhiyin Huang is a master student at Guangzhou University supervised by Prof. Siyu Ye. His main research interests are electrocatalysis, proton exchange membrane fuel cell, platinum-based catalyst support.

Junda Chen is currently a master student at Guangzhou University supervised by Prof. Siyu Ye. He received his B.E degree from Guangdong University of Technology. His research interests mainly focus on stable oxide catalysts and their applications in oxygen evolution reactions.

Yangdong Zhou is currently a Master student at Guangzhou University supervised by Prof. Siyu Ye. He received his B.E. degree from Qingdao University of Science and Technology. His research interest is focused on oxygen reduction reaction and ultra-low platinum and non-platinum coupling catalyst for fuel cell cathodes.

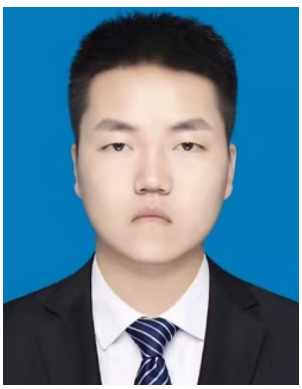

Puwei Wu is a master student in the materials engineering at Guangzhou University supervised by Prof. Siyu Ye. His main research interests include chemical conversion in electrocatalysis, mechanism and devices.

Ling Meng is a postdoctoral fellow in Prof. Siyu Ye's group at Guangzhou University. She received her PhD degree from South China University of Technology in 2021. In 2015, she was awarded the title of senior engineer in the field of light industry science and engineering. Her main research interests are high-performance paper-based composites, carbon-based porous materials and carbon–carbon composites, which are used in fuel cells, capacitors, lithium-ion batteries and sodium-ion batteries.

Ning Wang is currently an associate professor at Guangzhou University, China. She received her Ph.D. in Chemistry of Engineering from Hokkaido University, Japan. Her research interest mainly focuses on protonic conducting fuel cells, electrolysis cells, mixed ionic–electronic conductors, and machine learning accelerating the development of materials.

Lixin Xing is currently a lecturer at Guangzhou University. She received her Ph.D. degree at the year of 2016 from Harbin Institute of Technology. She was studying at the Pennsylvania State University as a visiting student directed by Prof. Qing Wang. Her research is focused on fundamental study and high-performance functional nanocomposite for electrochemical energy conversion and storage.

Mingquan Zhao received his master's degree from Xiamen university, China. He is currently a research & development engineer at SinoHyKey Technology Company Ltd. His research areas include catalyst layer design of PEMFCS, catalyst ink investigation, and coating technology development.

Yunsong Yang received his Ph.D. degree in polymer science and physics from Zhejiang University in 1998, followed by postdoctoral fellowships at Japan Science and Technology Agency (JST) and Simon Fraser University. He joined Ballard Power Systems (2007) and then automotive fuel cell corporation (AFCC) (2008) working on proton exchange membrane and MEA for PEM fuel cells. In 2018, he joined SinoHyKey Technology Company Ltd., as the director of the research and development department. He focuses on research and development of the MEA materials and catalyst layer designing for PEMFCS and PEMWES.

Junke Tang is the head of SinoHyKey's production operations. Prior to joining the company, Dr. Tang led the development of China's first polymer electrolyte membrane production line and has been awarded over fifty patents, eight of which are international. With his expertise in high precision, ultra-thin membrane technology, and its engineering processes, he has since come to establish SinoHyKey's roll-to-roll CCM coating line and make significant advancements in the commercialization of high-performance MEAs.

Yuquan Zou obtained his Ph.D. degree from the University of Singapore majoring in polymer chemistry. After his postdoctoral research at the University of British Columbia, Dr. Zou joined the automotive fuel cell corporation (AFCC) that was a joint venture between Daimler and Ford. His fuel cell expertise covers ionomer and membrane characterization, CCM design and manufacturing. He is currently CEO of SinoHyKey Technology Company Ltd.

Siyu Ye is a fellow of the Canadian Academy of Engineering, a professor at Guangzhou University, and a vice Chair and Chief Technology Officer at SinoHykey. He is recognized as a world-leading expert in electrocatalysis and catalyst layer/MEA design for fuel cells and water electrolysis, and has made significant contributions to the advancement of the modern protonic exchange membrane fuel cells and electrolysis cells.